JM PAPERS

Rotational dynamics of a neutrally buoyant prolate spheroid in viscoelastic shear flows at finite Reynolds numbers

Yansong Li[1], Chunxiao Xu[1] and Lihao Zhao[1],†

[1]AML, Department of Engineering Mechanics, Tsinghua University, Beijing 100084, PR China

Non-spherical particles exhibit peculiar behaviour in non-Newtonian flows. In this paper, we numerically investigate the dynamics of a neutrally buoyant prolate spheroid immersed in viscoelastic shear flows at finite Reynolds numbers by means of the immersed boundary method. Our results show that the period of particle rotation changes monotonically with the solvent viscosity ratio but non-monotonically with the mobility factor. Furthermore, we find five rotation modes of the spheroid under the effects of fluid inertia and fluid rheology in the present flow configuration. With weak fluid inertia, the particle rotation rate is remarkably reduced by fluid elasticity, which also induces asymmetric rotational behaviour. While the particle tends to tumble in the shear plane with weak fluid elasticity and moderate fluid inertia. However, as the fluid elasticity increases, the particle rotates with a newly observed mode, named the asymmetric-kayaking mode, which is classified by two additional critical elastic numbers that differ from the earlier studies on Stokesian viscoelastic shear flows. The present findings imply the importance of fluid inertia and fluid elasticity on the particle dynamics and could be potentially used to control the particle orientations in viscoelastic fluid flows.

Key words: particle/fluid flow, viscoelasticity

1. Introduction

Particle-laden flows of non-Newtonian fluids are widely encountered in the natural and industrial areas. Examples of these particle-laden non-Newtonian flows include fibre-reinforced polymers or rubbers (D'Avino & Maffettone 2015), red blood cell (RBC) transport in the vessels (Ye, Phan-Thien & Lim 2016; Beris *et al.* 2021), viscoelasticity-based cell separations in microfluidics (Lin & Huo 2015; D'Avino, Greco & Maffettone 2017; Li & Lin 2022), the fibre-like microorganisms swimming

† Email address for correspondence: zhaolihao@tsinghua.edu.cn

in non-Newtonian fluid environments (Storm *et al.* 2005; Li & Ardekani 2016), just to name a few. All these suspensions mentioned above can exhibit peculiar features, such as viscoelastic and shear-thinning effects. It is well known that these non-Newtonian characteristics can significantly influence the behaviour of particles in fluid flow. Needless to say, the particle dynamics will conversely affect the bulk properties of suspensions (Ngo, Nguyen & Oh 2021). Thus, from both the fundamental and the applied perspectives, understanding the dynamics of particles is important for designing and optimizing industrial applications involving non-Newtonian particulate two-phase flows. To uncover the statistical physics of the collective distribution and orientation of particles, it is, first of all, of importance to understand how a single particle orientates and rotates in non-Newtonian flows.

The particle dynamics in shear flows has been widely explored in previous studies. For a single particle rotation in an unconfined shear flow, Jeffery (1922) first derived the angular velocity of a non-spherical particle immersed in a simple shear flow of Newtonian fluid, ignoring both fluid and particle inertia. The results indicate that the particle rotates around the vorticity axis along different closed orbits (so-called Jeffery orbits) with different initial orientations. There exist abundant studies on the modulations of Jeffery orbits due to fluid or particle inertia (Taylor 1923; Saffman 1956; Lundell & Carlsson 2010). Rosén, Lundell & Aidun (2014) and Rosén *et al.* (2015*a*) conducted a systematic study on the effect of fluid inertia on the rotation mode of a neutrally buoyant particle with different Reynolds numbers. Besides the fluid and particle inertia, the rheological characteristic of the fluid flow is another factor affecting the particle rotation modes. Considering that viscoelasticity is a typical rheological characteristic of non-Newtonian fluids, the rotation modes of a single particle in viscoelastic fluids have long been actively investigated.

The studies on particle rotational dynamics in viscoelastic fluid flows began with spherical particles. When the elastic effect of fluid is weak, the theoretical results show that the particle angular velocity is almost unchanged in the second-order fluid (SOF, a kind of weakly viscoelastic fluid) (D'Avino & Maffettone 2015). However, when the particle is immersed in a fluid with strong viscoelasticity, both experimental and numerical results evidence that the fluid elasticity can dramatically slow down the particle rotation rate (Hwang, Hulsen & Meijer 2004; D'Avino *et al.* 2008; Snijkers *et al.* 2009; Housiadas & Tanner 2011; Snijkers *et al.* 2011). Snijkers *et al.* (2011) numerically explored the rotational dynamics of a spherical particle in the Oldroyd-B fluid, the results indicate that the closed orbits around the particle become distorted and form two recirculation regions, which are opposite to the primary flow.

Regarding non-spherical particles, researchers devoted efforts to investigating the rotational behaviours of ellipsoids in viscoelastic fluid flows by experiments. These experimental studies show that the viscoelasticity could significantly increase the particle rotational period (Gauthier, Goldsmith & Mason 1971). Apart from the particle rotation rates, the Jeffery orbits can also be affected by fluid rheology. Experiments, indeed, indicate that, when fluid elasticity is weak, the symmetry axis of rod-like particles eventually drifts to the vorticity direction, whereas it aligns in the shear plane for disk-like particles (Gauthier *et al.* 1971). However, moderate and strong fluid elasticities lead to distinct particle orientations, which have been demonstrated by experiments of red blood cell in a Boger fluid flow (Johnson, Salem & Fuller 1990). In moderately elastic fluids, it was observed that the ellipsoidal cells orientate between the vorticity and flow directions. In highly elastic fluids, the fibre-like particles align their symmetry axes along the flow direction (Iso, Cohen & Koch 1996*a*; Iso, Koch & Cohen 1996*b*). Later, several

more detailed experiments were conducted to analyse the effect of a wide range of fluid elasticities on the orientations of ellipsoids with different shapes (aspect ratio ranges from 2.0 to 8.0) (Gunes *et al.* 2008). Besides the aforementioned particle orientations in weakly and highly elastic fluids, there exists a more interesting particle orientation mode characterized by the bimodal distribution in a viscoelastic shear flow with a specific range of Deborah numbers (Gunes *et al.* 2008).

As for the theoretical studies, Leal (1975) derived an asymptotic solution for a rod-like particle immersed in the shear flow of a SOF fluid. The orientation modes predicted by the theoretical model are consistent with the experiments: rod-like particles evolve towards the vorticity axis in shear flows with low Deborah number, while they align along the flow direction in high Deborah number flow. Brunn (1977) further extended the theoretical model to the ellipsoids with other aspect ratios. Moreover, Dabade, Marath & Subramanian (2015) proposed a viscoelastic torque model based on the generalized reciprocal theorem. This model predicts the longside-on orientation for both prolate and oblate particles in the uniform flow of viscoelastic fluids, in which the first normal stress difference of fluid is positive and dominant.

Considering the limitation of the small expansion parameters used in the asymptotic theory, theoretical studies are mainly restricted to weakly viscoelastic fluids, such as a SOF. The results predicted by this theorem could not reveal the more complex orientation modes (such as the orientation between the vorticity and flow directions) observed in experiments. In addition, the theoretical approaches also could not be used to handle the more realistic fluids described by the highly nonlinear constitutive equations, such as the Giesekus model. Thus, to understand the mechanisms of the particle behaviours in fluid flows with more complex rheological properties, numerical approaches are needed. Numerical simulations of the rotational dynamics of ellipsoids in viscoelastic shear flows have received extensive attention (Phan-Thien & Fan 2002; Nguyen-Hoang *et al.* 2008; Wang, Yu & Lin 2019). D'Avino *et al.* (2014) and D'Avino, Greco & Maffettone (2015) systemically analysed the detailed dynamics of prolate particles in a sheared Giesekus fluid by finite element simulations. Due to the fluid elasticity, the particle rotation could be categorized into four different modes: (i) in low Deborah number flow, the prolate particles align their symmetry axes along the vorticity direction and behave in a 'log-rolling' mode. (ii) With increasing shear rate or fluid elasticity, the particles drift towards the shear plane and finally align between the flow and vorticity directions. (iii) When the Deborah number reaches a critical threshold value, an interesting bi-stable orientation mode appears. In this rotation mode, the final equilibrium state of a particle depends upon its initial orientations. (iv) Finally, in highly elastic flow with large Deborah number, the particles eventually align with the flow direction.

To summarize, although there are a few studies on the rotational dynamics of non-spherical particles in viscoelastic flows, these studies are mostly confined to flows which are fluid elasticity dominated, where the fluid and particle inertia are both absent. The interplay between fluid elasticity and inertial effects on particle behaviours in shear flows is not yet explored. The elasto-inertial coupling effect is expected to affect the particle dynamics. For example, induced by the competition between fluid inertia and elasticity, the particles exhibit a different lateral migration in duct flows (Li, McKinley & Ardekani 2015; Yu *et al.* 2019). However, in viscoelastic flows with fluid inertia, the research on this coupling effect on particle rotational behaviours is still developing.

The main dimensionless numbers governing the particle dynamics in viscoelastic flows include the Reynolds number, *Re*, Stokes number, *St* and Weissenberg, *Wi* or Deborah

number, *De*. The previous studies are mostly confined to inertia-free particles immersed in viscoelastic flows within the Stokesian regime, i.e. *Re*, *St* ∼ 0 and *Wi* or *De* > 0. From this point of view, there exist gaps in the parameter space, where fluid inertia, particle inertia and fluid elasticity coexist in the suspension system (*Re* > 0, *St* > 0, *Wi* or *De* > 0). The present research aims at mapping the parameter space and understanding the influences of the controlling parameters on the particle rotational dynamics in viscoelastic flows. Besides the above potential fundamental contributions, it is also of practical importance to study the particle rotation in viscoelastic–inertial shear flows. One of the popularly used techniques to improve the efficiency of particle separation in microfluidics is using viscoelastic liquids with low viscosity and high elasticity (Lu & Xuan 2015; Li *et al.* 2015; D'Avino *et al.* 2017; Raoufi *et al.* 2019). In this regard, both fluid inertia and elasticity are important to the particle behaviours. Therefore, studying the elasto-inertial orientation of particles is instrumental in optimizing particle manipulation in microfluidic applications. Considering that viscoelastic-based particle manipulation is mainly utilized in biomedical areas, particles (such as RBC) are nearly neutrally suspended in the background fluids. The densities of these particles are generally similar to those of suspension fluids (Atwell *et al.* 2022). Thus, the present study mainly focuses on neutrally buoyant particles. Moreover, the prolate spheroids suspended in viscoelastic fluids are widely encountered in various engineering applications, such as fibre-reinforced composite materials (Altan 1990; Nabergoj, Urevc & Halilovič 2022), papermaking processes (Lundell, Söderberg & Alfredsson 2011) and the 'rouleaux' structure (a prolate spheroidal microstructure of RBCs) in blood (Fedosov *et al.* 2011; Kang 2002). The orientation modes of these elongated particles can significantly affect the bulk properties of polymeric suspensions. This motivates the present study on the rotational dynamics of neutrally buoyant prolate spheroids in viscoelastic shear flows.

Finally, the particle shape and the characteristics of the particle surface also greatly affect the particle rotation in shear flows. For example, the critical Weissenberg numbers for the transition of the spheroid rotation modes are decreased by the particle aspect ratio (Gunes *et al.* 2008). Oblate spheroids behave differently with prolate spheroids in Newtonian (Rosén *et al.* 2015*b*) and viscoelastic (Gauthier *et al.* 1971) shear flows. For a more complicated case, i.e. particles with irregular shapes, Daghooghi & Borazjani (2018) found that the periodicity of the angular velocity could be broken by the non-asymmetry of irregularly shaped particles. This implies that the rotational dynamics of particles can be greatly altered by the particle shape. As for particles with a non-smooth surface, the local flow field near the particle surface is sensitive to the characteristics of the particle surface. Liu *et al.* (2020) indicated that the rotation periods of highly permeable elliptical particles are smaller than those of particles with smaller porosity. In this case, the porous effect on the flow field should also be considered in the governing equations of fluid flow. Note that the coupled effect of fluid inertia and fluid elasticity on the rotation modes of the above complex spheroids should be studied based on the systematic knowledge of the single effect, which, however, is still developing. Considering this, the effects of particle shape and surface characteristics on particle rotational dynamics deserve to be studied in detail in future work.

The work is organized as follows. In § 2, we introduce the mathematical models and numerical methods for resolving the viscoelastic flow and particle rotation. Then the modulations of the three-dimensional (3-D) rotation modes by the interplay between fluid elasticity and inertial effects are analysed in § 3. Finally, conclusions are drawn in § 4.

2. Mathematical models and numerical methods

2.1. *Governing equations*

The mathematical models describing the present problem consist of the governing equations for viscoelastic fluid flow and particle rotation.

2.1.1. *Viscoelastic fluid flow*

For the fluid phase, the governing equations for incompressible and isothermal viscoelastic flows are written as

$$\nabla \cdot \boldsymbol{u} = 0, \tag{2.1}$$

$$\rho_f \left(\frac{\partial \boldsymbol{u}}{\partial t} + \boldsymbol{u} \cdot \nabla \boldsymbol{u} \right) = -\nabla p + \nabla \cdot \boldsymbol{\tau}^s + \nabla \cdot \boldsymbol{\tau}^p + \boldsymbol{f}^{IB}, \tag{2.2}$$

where $\boldsymbol{u}$ is the fluid velocity, ρ_f is the fluid density, p is the pressure and $\boldsymbol{f}^{IB}$ is the momentum force due to the fluid–particle interaction. To improve the computational stability of the viscoelastic flow simulation, the total stress is decomposed into the polymeric stress $\boldsymbol{\tau}^p$ and the solvent stress $\boldsymbol{\tau}^s$ (Alves, Oliveira & Pinho 2021).

Generally, the solvent stress of viscoelastic fluid can be written as

$$\boldsymbol{\tau}^s = \mu_s \left(\nabla \boldsymbol{u} + (\nabla \boldsymbol{u})^{\mathrm{T}} \right). \tag{2.3}$$

The zero-shear-rate viscosity μ_0 and the solvent viscosity ratio β are defined as follows:

$$\mu_0 \equiv \mu_s + \mu_p, \tag{2.4a}$$

$$\beta \equiv \frac{\mu_s}{\mu_0}, \tag{2.4b}$$

where μ_s and μ_p represent the solvent and polymeric contributions to the zero-shear-rate viscosity, respectively.

The polymer stress can be further formulated as the following constitutive equation:

$$\boldsymbol{\tau}^p + \lambda \left(\frac{\partial \boldsymbol{\tau}^p}{\partial t} + \boldsymbol{u} \cdot \nabla \boldsymbol{\tau}^p - \boldsymbol{\tau}^p \cdot \nabla \boldsymbol{u} - (\nabla \boldsymbol{u})^{\mathrm{T}} \cdot \boldsymbol{\tau}^p + \frac{\alpha}{\mu_p} \boldsymbol{\tau}^p \cdot \boldsymbol{\tau}^p \right) = \mu_p \left(\nabla \boldsymbol{u} + (\nabla \boldsymbol{u})^{\mathrm{T}} \right), \tag{2.5}$$

where λ is the polymer relaxation time and α denotes the mobility factor representing the shear-thinning rheology of the polymeric solution. For a Giesekus-type fluid, the larger the mobility factor is, the more appreciable is the shear-thinning effect of the fluid; it is normally less than 0.5 to avoid unphysical solutions (Alves *et al.* 2021). Specifically, (2.5) reduces to the Oldroyd-B model when $\alpha = 0$.

The polymer stress in the Oldroyd-B and Giesekus models can be determined by the conformation tensor $\boldsymbol{B}$ based on the kinetic theory as

$$\boldsymbol{\tau}^p = \frac{\mu_p}{\lambda} \left(\boldsymbol{B} - \boldsymbol{I} \right), \tag{2.6}$$

where $\boldsymbol{I}$ is the identity matrix.

Then the conformation tensor-form constitutive equation can be described as

$$\frac{\partial \boldsymbol{B}}{\partial t} + \boldsymbol{u} \cdot \nabla \boldsymbol{B} - \boldsymbol{B} \cdot (\nabla \boldsymbol{u}) - (\nabla \boldsymbol{u})^{\mathrm{T}} \cdot \boldsymbol{B} = \frac{1}{\lambda} \left[\boldsymbol{I} - \boldsymbol{B} - \alpha \left(\boldsymbol{B} \cdot \boldsymbol{B} - 2\boldsymbol{B} + \boldsymbol{I} \right) \right]. \tag{2.7}$$

2.1.2. *Particle rotation*

Concerning the particle rotational motion, the following Euler equation is utilized:

$$\frac{\mathrm{d}\left(I_p\boldsymbol{\omega}_p\right)}{\mathrm{d}t} = \oint_{\Gamma_p} \boldsymbol{r} \times (\boldsymbol{\tau} \cdot \boldsymbol{n}) \,\mathrm{d}s, \tag{2.8}$$

where $\boldsymbol{I}_p$ is the particle moment of inertia, $\boldsymbol{\omega}_p$ represents the particle angular velocity, Γ_p is the particle surface, $\boldsymbol{r}$ is the position vector on the particle surface from the particle centre and $\boldsymbol{n}$ denotes the unit normal vector pointing outwards on the particle surface; $\boldsymbol{\tau}$ represents the hydrodynamic stress tensor acting on the particle as $\boldsymbol{\tau} = -p\boldsymbol{I} + \boldsymbol{\tau}^s + \boldsymbol{\tau}^p$. The integration of $\boldsymbol{\tau}$ accounts for the fluid–particle interaction

The immersed boundary method (IBM) is capable of resolving the effects of finite fluid inertia and fluid elasticity on particle rotation. Therefore, IBM is adopted to model the viscoelastic fluid–particle interaction in the present study. By integrating the momentum equation (2.2) and the Gauss theorem, the hydrodynamic torque acting on the particle can be rewritten as

$$\oint_{\Gamma_p} \boldsymbol{r} \times (\boldsymbol{\tau} \cdot \boldsymbol{n}) \,\mathrm{d}s = \int_{\Omega_p} \boldsymbol{r} \times (\boldsymbol{\nabla} \cdot \boldsymbol{\tau}) \,\mathrm{d}v = \frac{\mathrm{d}}{\mathrm{d}t} \int_{\Omega_p} \rho_f \boldsymbol{r} \times \boldsymbol{u} \,\mathrm{d}v - \int_{\Omega_p} \boldsymbol{r} \times \boldsymbol{f}^{IB} \,\mathrm{d}v, \tag{2.9}$$

where Ω_p is the particle region bounded with surface Γ_p. In IBM, the momentum forcing term $\boldsymbol{f}^{IB}$ in (2.2) and (2.9) is used to satisfy the no-slip condition on the particle surface, which is spread from the fluid–particle interaction forcing term $\boldsymbol{F}_{IB}$

$$\boldsymbol{f}^{IB} = \oint_{\Gamma_p} \boldsymbol{F}_{IB}\delta(\boldsymbol{x} - \boldsymbol{X}) \,\mathrm{d}s, \tag{2.10}$$

where δ is the Dirac delta function. Here, $\boldsymbol{X}$ denotes the positions of material Lagrangian points distributed on the particle surface. In the penalty IBM, the fluid–particle interaction forcing term $\boldsymbol{F}_{IB}$, acting on the particle surface from the fluid, is given as (Huang, Chang & Sung 2011)

$$\boldsymbol{F}_{IB} = -\kappa \left[(\boldsymbol{X}_{IB} - \boldsymbol{X}) + \Delta t\,(\boldsymbol{U}_{IB} - \boldsymbol{U})\right], \tag{2.11}$$

where κ is a large penalty constant in IBM with $\kappa = 10^4$ in the present simulations; $\boldsymbol{X}_{IB}$ and $\boldsymbol{U}_{IB}$ represent the positions and velocities of the massless counterparts of the material Lagrangian points, respectively, and $\boldsymbol{U}$ denotes the velocities of the material Lagrangian points; Δt is the time step.

To elaborate on the elasto-inertial effect on the particle rotational dynamics, the particle is fixed at the centre of the simulation domain, thus the translation of particles is neglected in this study. However, the particle rotation is not constrained, and the particle can freely rotate in all directions. The flow configuration investigated in the present work is sketched in figure 1, and the corresponding non-dimensional parameters are summarized as follows:

  (i) Particle Reynolds number, $Re_p = GD_p^2/\nu_0$, where G is the constant shear rate of the flow, D_p is the characteristic length of the particles, i.e. the major diameter of the particles, and ν_0 is the zero-shear-rate kinematic viscosity of viscoelastic fluids. In the present simulation, the fluid shear rate G and particle major-axis diameter D_p are set as $G = 1.0$ and $D_p = 1.0$, respectively. The effect of fluid inertia is represented by the variation of the zero-shear-rate kinematic viscosity ν_0.

  (ii) Stokes number, $St = \rho_r Re_p$, which represents particle inertia. Here, ρ_r is the ratio between the particle and fluid densities, $\rho_r = \rho_p/\rho_f$. In the present work, we focus on neutrally buoyant particles, i.e. $\rho_r = 1.0$, and thus $St = Re_p$.
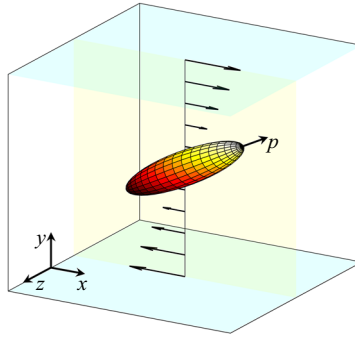
Figure 1. Schematic of a prolate spheroid in a viscoelastic shear flow.

(iii) Weissenberg number, $Wi = \lambda G$, which represents the elastic effect of fluids.
(iv) Elastic number, $El = Wi/Re_p$, which quantifies the competition between fluid elastic and fluid inertial effects.
(v) Particle aspect ratio, $AR = a/b$, where a and b are the polar and equatorial radii of a spheroid, respectively.

2.2. *Numerical methods*

2.2.1. *Viscoelastic flow solver*

The governing equations of a viscoelastic fluid are discretized on the staggered grid using a finite-difference method. The pressure and conformation tensor are defined on the cell centre, while the velocity is located on the centre of the cell face, which is orthogonal to its stored velocity component. For spatial discretization of the governing equations, all terms are approximated by the second-order central difference scheme, except for the convective term in the constitutive equation, which is evaluated by a high-resolution scheme, i.e. the CUBISTA scheme that is often used in viscoelastic flow simulations (Pimenta & Alves 2017). For temporal discretization of the momentum and constitutive equations, all terms are integrated in time by the second-order Crank–Nicolson scheme. The incremental form and staggered time (ST) scheme are utilized to treat the pressure gradient and elastic stress terms. In the ST scheme, the velocity was defined at the n time level while the pressure and conformation tensor were defined at the $n + 1/2$ time level. More details on the numerical method can be found in Li *et al.* (2022). With the above temporal and spatial discretization schemes, the discretized governing equations of viscoelastic flow can be written as

$$D\boldsymbol{u}^{n+1} = cbc^n, \tag{2.12}$$

$$\frac{\boldsymbol{u}^{n+1}}{\Delta t} + N\boldsymbol{u}^{n+1} - \frac{\beta}{2Re}L\boldsymbol{u}^{n+1} + G_f\delta p - \frac{1-\beta}{WiRe_p}D\delta\boldsymbol{B}$$
$$= \frac{\boldsymbol{u}^n}{\Delta t} - G_f p^{n-1/2} + \frac{\beta}{2Re}L\boldsymbol{u}^n + \frac{1-\beta}{WiRe_p}D\boldsymbol{B}^{n-1/2} + \boldsymbol{mbc}^{n+1/2} + \boldsymbol{f}^{IB,n+1/2}, \tag{2.13}$$

$$\frac{\delta\boldsymbol{B}}{\Delta t} + \frac{1}{2}N_u\delta\boldsymbol{B} + N_u\boldsymbol{B}^{n-1/2} - \frac{1}{2}\delta\boldsymbol{B} \cdot (G_f\boldsymbol{u}^n) - \boldsymbol{B}^{n-1/2} \cdot (G_f\boldsymbol{u}^n)$$
$$- \frac{1}{2}(G_f\boldsymbol{u}^n)^{\mathrm{T}} \cdot \delta\boldsymbol{B} - (G_f\boldsymbol{u}^n)^{\mathrm{T}} \cdot \boldsymbol{B}^{n-1/2}$$

$$+ \frac{1}{2Wi} \delta \boldsymbol{B} + \frac{\alpha}{2Wi} \left(\delta \boldsymbol{B} \cdot \boldsymbol{B}^{n-1/2} + \boldsymbol{B}^{n-1/2} \cdot \delta \boldsymbol{B} - 2\delta \boldsymbol{B} \right)$$

$$= \frac{1}{Wi} \left(\boldsymbol{I} - \boldsymbol{B}^{n-1/2} \right) - \frac{\alpha}{Wi} \left[\boldsymbol{B}^{n-1/2} \cdot \boldsymbol{B}^{n-1/2} - 2\boldsymbol{B}^{n-1/2} + \boldsymbol{I} \right], \qquad (2.14)$$

where $\delta p = p^{n+1/2} - p^{n-1/2}$, $\delta \boldsymbol{B} = \boldsymbol{B}^{n+1/2} - \boldsymbol{B}^{n-1/2}$, *cbc* is the discretization of the boundary condition in the continuity equation and **mbc** is the discretization of the boundary condition in the momentum equation. Further, D represents the discretized divergence operator, N represents the coefficient matrix of $\boldsymbol{u}^{n+1}$ in the discretized convective term of the momentum equation, G_f denotes the discretized gradient operator, L represents the discrete Laplacian operator and N_u denotes the coefficient matrix of $\boldsymbol{B}$ in the discretized convective term of the constitutive equation. Note that there is no need to prescribe a boundary condition for the constitutive equation.

By rearranging the discretized governing equations (2.12)–(2.14) in a monolithic matrix system, the pressure, conformation tensor and velocity can be decoupled from the viscoelastic flow system sequentially based on the approximate factorization of the system coefficient matrix. This decoupling procedure has been successfully applied to Newtonian (Kim, Baek & Sung 2002; Pan, Kim & Choi 2019) and viscoelastic (Li *et al.* 2022) flow simulations. With this method, all quantities can be resolved in a projection framework without iteration.

2.2.2. *Particle solver*

For the particle phase, substituting equation (2.9) and (2.10) into the particle governing equation (2.8), the rotation of a particle is further described as follows:

$$\frac{\mathrm{d} \left(I_p \boldsymbol{\omega}_p \right)}{\mathrm{d}t} \approx - \sum_{l}^{N_l} \boldsymbol{r} \times \boldsymbol{F}_{IB,l} \Delta s_l + \rho_f \frac{\mathrm{d}}{\mathrm{d}t} \left(\int_{\Omega_p} \boldsymbol{r} \times \boldsymbol{u} \, \mathrm{d}v \right), \qquad (2.15)$$

where Δs_l is the surface area of each Lagrangian element on the particle surface and N_l is the total number of Lagrangian points.

The discretized particle rotation equation (2.15) is solved in the particle frame with the fourth-order Runge–Kutta scheme. The particle orientation is represented by quaternions (Goldstein 1980), which are updated based on the particle angular velocity.

In the present study, the particle is located at the centre of a box with a size of $L \times H \times W$. The top and bottom boundaries of the computational domain move with a constant velocity in opposite directions. The velocity distribution of a simple shear flow is applied at the inlet boundary. Considering the fluid inertial effect, the convective outflow boundary is set at the outlet of the computational region. The periodic boundary is set in the spanwise direction. The size of the computational domain could affect the particle rotation in shear flows, thus, we compared the results calculated in the different computational domains to examine the domain-size effect on the particle rotation, as shown in figure 2. It can be seen that the evolutions of particle orientation and angular velocity calculated with two larger domains are in good agreement, while the results obtained using the small domain deviate slightly. Considering the computational cost, the domain size of $L \times H \times W = 8 \times 8 \times 4$ is chosen in the following simulations. The number of Eulerian grid points per major diameter of the particle is 32, thus the mesh resolution is $\Delta = 1/32$. The time step is set as $\Delta t = 10^{-3}$ in all simulations. With this time step, the Courant–Friedrichs–Lewy numbers in all simulations satisfy $\max\{u\Delta t/\Delta, v\Delta t/\Delta x, w\Delta t/\Delta\} \leqslant 0.2$, where u, v, w
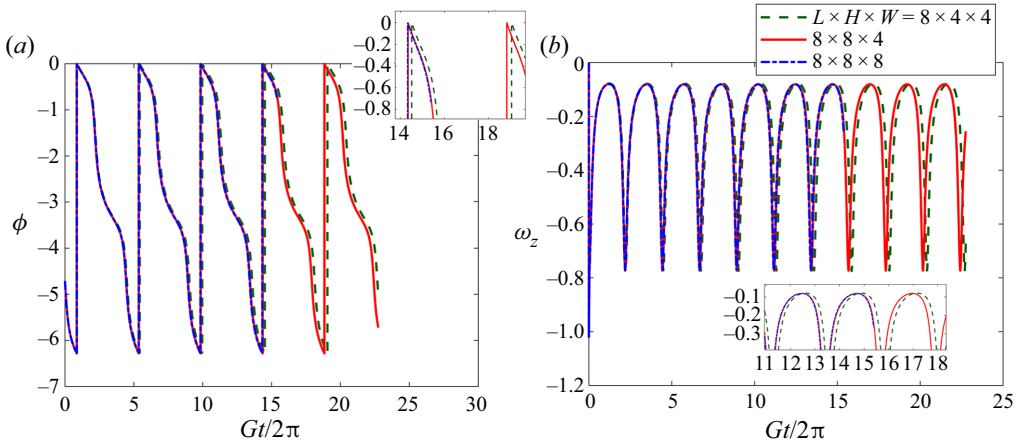
958 A20-8

Figure 2. Comparisons of (*a*) azimuthal angle and (*b*) angular velocity vs time for a prolate with $AR = 2.0$, $Re_p = 0.1$ and $Wi = 2.0$ in different computational domain sizes.

denote three velocity components in the flow field. The validation of the present numerical methods is presented in Appendix A.

3. Results and discussion

As mentioned in §1, the single effect of fluid inertia or fluid elasticity on the rotation of prolate spheroids has been extensively studied. For fluid inertia, the orientation modes of prolate spheroids with $AR = 2$ (Yu, Phan-Thien & Tanner 2007; Huang *et al.* 2012) and $AR = 4$ (Rosén *et al.* 2014) have been comprehensively analysed in Newtonian shear flows. In Stokesian viscoelastic shear flows, the rotational dynamics of prolate spheroids ($AR = 4$) is also reported in simulations (D'Avino *et al.* 2014) and experiments ($AR = 2 \sim 6$) (Johnson *et al.* 1990). To clearly elaborate on the different orientation modes of prolate spheroids induced by the elasto-inertial effect, we focus on the prolate spheroids with the same aspect ratios ($AR = 1$, 2 and 4) used in the earlier studies on the single effect.

Considering the finite fluid inertia in the practical applications related to the dynamics of particles in viscoelastic fluids, we set the particle Reynolds number as $Re_p = 0.1$ and $Re_p = 10.0$ in the present study. These specific values of Re_p are chosen mainly for the fluid inertia in the manipulation of bioparticles in microfluidics. Lu & Xuan (2015) and Lim *et al.* (2014) experimentally studied the elasto-inertial focusing of particles in viscoelastic flows with different fluid inertia, i.e. bulk Reynolds numbers $Re_H = UH/\nu_0 = 4.86$ and 105.0 (*U* is the bulk velocity and *H* denotes the height of microchannel). Correspondingly, the shear Reynolds numbers of particles in their experiments are roughly estimated as Re_p about $O(0.1) \sim O(10.0)$. Thus, the present study mainly focuses on the cases with weak and moderate fluid inertia, i.e. $Re_p = 0.1$ and $Re_p = 10.0$.

In this section, the rotational dynamics of particles in viscoelastic shear flows with finite fluid inertia is investigated numerically. To investigate the effect of fluid elasticity on the particle rotation in the shear plane, we first focus on the case with weak fluid inertia ($Re_p = 0.1$) in §3.1. Then, with moderate fluid inertia ($Re_p = 10.0$), the orientation modes and drift of particle 3-D orbits induced by the competition between fluid elasticity and fluid inertial effects are studied in §3.2.
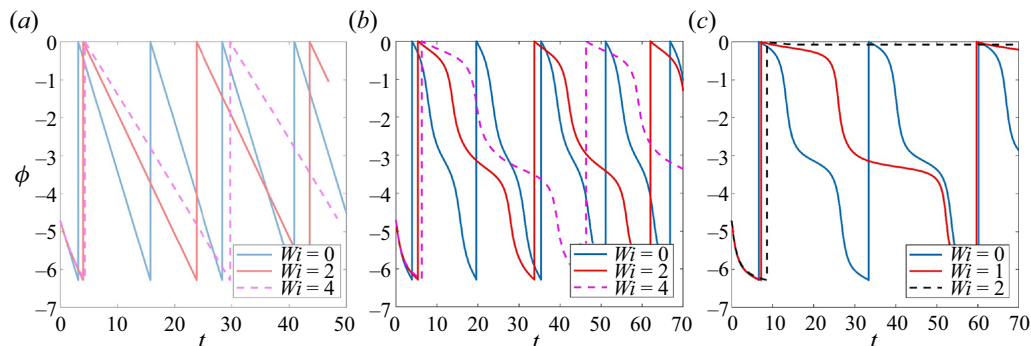
Figure 3. Evolution of azimuthal angle of particle with different aspect ratios: (*a*) $AR = 1.0$; (*b*) $AR = 2.0$; (*c*) $AR = 4.0$.
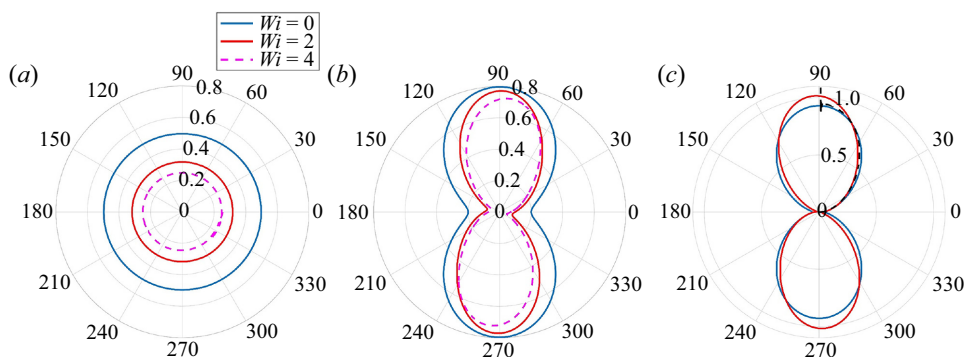

Figure 4. Particle angular velocity vs orientation in the polar coordinate system. The radial coordinate represents particle angular velocity and the polar angle denotes the azimuthal angle between the particle symmetry axis and the streamwise direction: (*a*) $AR = 1.0$; (*b*) $AR = 2.0$; (*c*) $AR = 4.0$.

3.1. *Particle rotation in the shear plane*

3.1.1. *Effect of fluid elasticity*

To understand the mechanism of the reduction of the particle rotation rate caused by fluid elasticity, we look into the viscoelastic shear flow with weak fluid inertia ($Re_p = 0.1$). The rheological parameters in the present viscoelastic shear flows are set as $\beta = 0.0909$ and $\alpha = 0.2$, which are consistent with those in the earlier work (D'Avino *et al.* 2014). The evolutions of the azimuthal angle of prolate spheroids are shown in figure 3, in which, compared with the Newtonian case ($Wi = 0$), fluid elasticity significantly increases the particle rotation period in viscoelastic flows. The rotation period of particles with large aspect ratios is more obviously changed by fluid elasticity. For $AR = 4.0$, the particle can remain in a motionless state, which reveals that fluid elasticity stabilizes the particle rotation. In addition, we further analyse the effect of fluid elasticity on the particle angular velocity at different orientations, and the results are shown in figure 4.

For spherical particles, figure 4 suggests that spherical particles rotate with a constant angular velocity in viscoelastic fluids, which is similar to that in a Newtonian case. The sphere rotation rate is remarkably reduced by fluid elasticity, which is consistent with the results reported by Snijkers *et al.* (2011), and spheroidal particles exhibit more peculiar rotation behaviours in viscoelastic shear flows. The particles with different
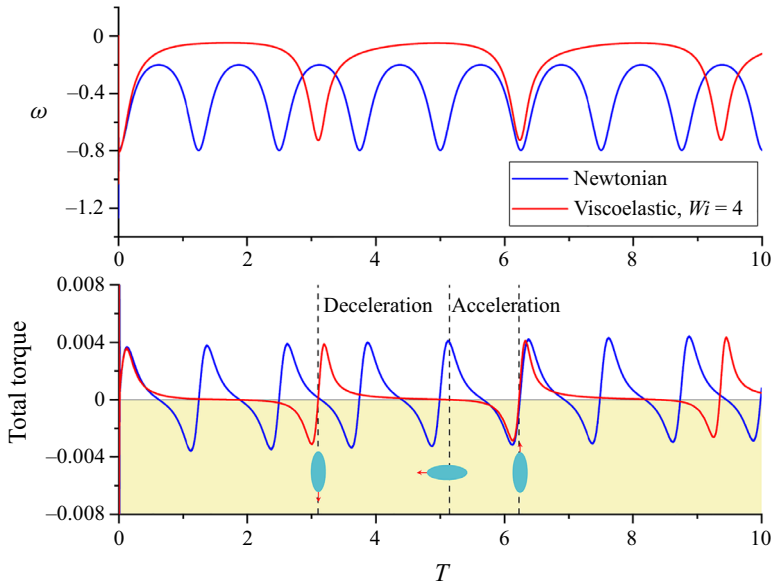
958 A20-10

Figure 5. Evolution of total hydrodynamic torque acting on a particle with $AR = 2.0$. The torque in the shaded area represents the driving torque for particle rotation. $T = Gt/2\pi$.

aspect ratios are affected by fluid elasticity in different ways. For particles with small eccentricity ($AR = 2.0$), figure 4(b) shows that the curve of the particle angular velocity at different orientations in a stronger viscoelastic fluid ($Wi = 4$) is bounded by that in a weaker viscoelastic fluid ($Wi = 2$). This reveals that the particle angular velocities at all orientations are decelerated by fluid elasticity. However, for particles with large eccentricity ($AR = 4.0$), the influence of fluid elasticity on the particle angular velocity becomes orientation dependent. When the particle orients toward the flow direction, the particle angular velocity is slightly decreased by fluid elasticity, while it is increased when the particle is normal to the flow direction (seen in figure 4c). More interestingly, when the fluid elasticity further increases, the particle with $AR = 4.0$ reaches a steady alignment in the streamwise direction.

Figure 5 shows the variations of total torque during the particle rotation. It can be seen that fluid elasticity breaks the symmetry of the particle rotation process observed in Newtonian flow (blue line in figure 5). The particle deceleration takes a longer time than the acceleration. More quantitatively, the period of particle deceleration is approximately twice that of acceleration, which could be caused by the coupled effect of stress relaxation and the transient shear-thinning rheology (Varchanis *et al.* 2022) of viscoelastic fluids. During the particle deceleration, the local shear rate on the particle increases, except for the tip area of the particle. With the transient shear-thinning effect, the decreased local viscosity near the particle would lead to an attenuated drag force (less energy) on the particle from the surrounding fluids, and thus the particle rotation rate is hindered during its deceleration. This will strengthen the symmetry breaking of the particle rotation process.

Based on the kinematic theory, the conformation tensor $\boldsymbol{B}$ is defined as (Bird *et al.* 1987)

$$\boldsymbol{B} = \frac{\langle \boldsymbol{Q}\boldsymbol{Q} \rangle}{Q_{eq}^2}, \tag{3.1}$$
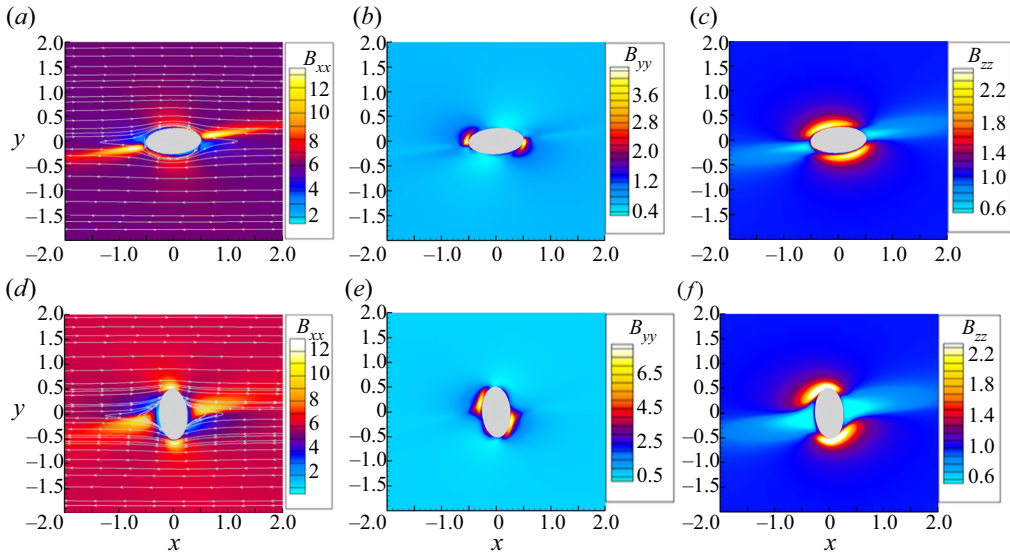
958 A20-11

Figure 6. Contour of conformation tensor around particle with $Wi = 4.0$, $AR = 2$: (*a*) and (*d*) B_{xx}; (*b*) and (*e*) B_{yy}; (*c*) and (*f*) B_{zz}.

where $\boldsymbol{Q}$ is the end-to-end vector in the dumbbell model of polymer molecules, and $\boldsymbol{Q}_{eq}$ represents $\boldsymbol{Q}$ at the polymer equilibrium state. From (3.1), the conformation tensor can quantify the relative deformation of the polymer molecule in the flow field.

According to the conformation tensor field shown in figure 6, it is found that the polymer deformation induced by the flow field depends on the particle orientation. When the particle symmetry axis changes from being perpendicular (*y* axis) to parallel (*x* axis) to the flow direction, B_{ii} becomes smaller. This represents the deformation of polymer being reduced and partially recovered (3.1) when the particle aligns its symmetry axis along the flow direction. The elastic torque acting on the particle is associated with the polymer deformation (as shown in (2.6)), thus the elastic stress will decrease during the particle deceleration process. However, the stress relaxation effect (due to the relaxation time λ) of the viscoelastic fluid makes the response of the elastic stress hysteretic to the strain variation (Ewoldt & Saengow 2022). Therefore, the decay of the elastic stress is retarded to the recovery of deformed polymer. Such a decaying characteristic of the elastic stress makes the particle experience a longer period of resisting hydrodynamic torque, thus the particle angular velocity evolves asymmetrically, as shown in figure 5.

Physically, the polymer is generally stretched in shear flows and forms stretched microstructures (seen in figure 6) in the flow field; these microstructures of polymer would create tension along the streamlines (Ewoldt & Saengow 2022). By comparing the distributions of the conformation tensor around particles with different orientations in figure 6, we find that the deformation of polymer is more obvious when the particle is perpendicular to the flow direction. This indicates that it is more difficult for particles to overcome the streamline tension when they are perpendicular to the flow direction. Thus, the orientation-dependent polymer deformation might also bring asymmetry to the particle rotation process shown in figure 5.

On the other hand, the reduction of the particle rotation rate in viscoelastic shear flows is also linked to the above stretched structure of polymer in the flow field. From figure 6, it is found that the maximum of the conformation tensor (B_{xx} in figure 6*a,d*) mainly locates around the particle tip. The distribution of the conformation tensor shows the 'sheet-like'
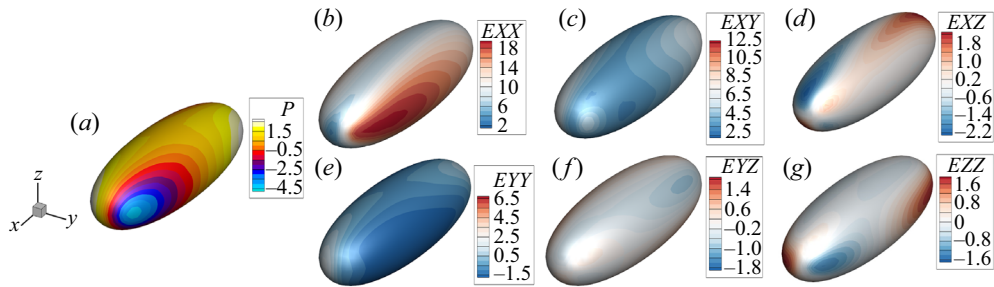
958 A20-12

Figure 7. Pressure and elastic stress contours on the particle surface ($Wi = 4.0$, $AR = 2$): (*a*) pressure; (*b*–*g*) the six independent components of the elastic stress tensor.

structure of polymer deformation in the particle upstream, especially for the distribution of B_{xx} in figure 6(*a*). Additionally, figure 7 shows the distribution of elastic stress on the particle surface when the particle aligns along the flow direction. Similar to figure 6, the strong elastic stress also mainly locates near the particle tip. The above distributions of the conformation tensor and elastic stress reveal that the polymer is highly stretched near the particle tip. When the particle rotates, the streamlines near the particle surface will be changed, and the streamline tension generated by the stretched structures of polymer induce an opposite torque to hinder the particle rotation, causing a reduction of the particle rotation rate in viscoelastic shear flows, as shown in figures 4 and 5.

3.1.2. *Effect of solvent viscosity ratio and mobility factor*

In addition to the effect of fluid elasticity (*Wi*), other rheological factors, including the solvent viscosity ratio and the mobility factor, also affect the flow characteristics and particle dynamics.

Figure 8 shows the particle angular velocities in viscoelastic shear flows with different solvent viscosity ratios. The solvent viscosity ratio reflects the contribution of solvent to the total zero-shear-rate viscosity of the viscoelastic fluid solution. From (2.6), it can be found that the smaller the solvent viscosity ratio is, the stronger the elastic stress is. Figure 8(*a*) indicates that the solvent viscosity ratio has little influence on the relationship between particle angular velocity and orientation. However, figures 8(*b*) and 8(*c*) obviously show that the evolutions of particle orientation and angular velocity can be changed by the solvent viscosity ratio. Figure 8(*b*) shows that the particle rotation period decreases monotonically with the viscosity ratio. With increasing solvent viscosity ratio, the elastic stress becomes weaker, and the particle angular velocity increases, thus the period of particle rotation decreases.

Compared with the influence of fluid elasticity (*Wi*) on the particle angular velocity (figure 5), the solvent viscosity ratio shows a more peculiar effect. From figure 8(*c*), we find that, with increasing solvent viscosity ratio, the magnitude of the maximum angular velocity decreases, while that of the minimum angular velocity increases.

Moreover, the shear-thinning and extension-hardening rheology, as two additional important rheological characteristics of polymeric solution, can be described by the Giesekus model. Previous studies have shown that the migration dynamics of particles is strongly affected by the mobility factor (Li *et al.* 2015). In this paper, we examine the effect of the mobility factor on the particle rotation behaviour, as shown in figure 9.

From figures 9(*a*) and 9(*c*), it is found that the mobility factor mainly affects the maximum angular velocity of the particle. Specifically, the magnitude of the maximum angular velocity is attenuated by the mobility factor, while the minimum angular velocity
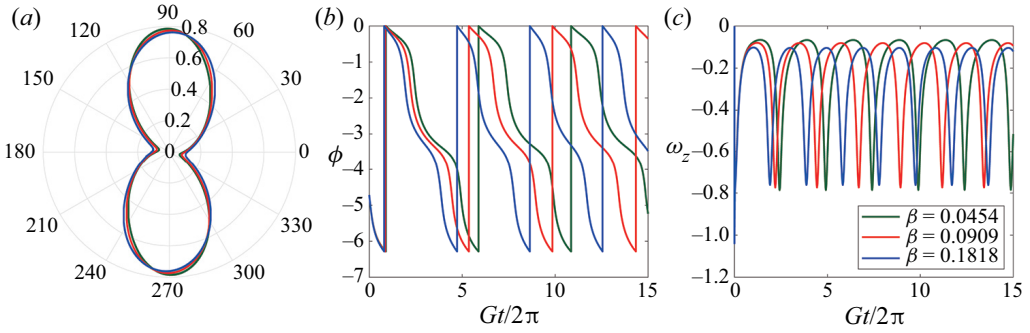
Figure 8. Effect of solvent viscosity ratio on particle rotation ($Wi = 2.0$, $AR = 2.0$): (*a*) angular velocity vs particle orientation; (*b*) azimuthal angle; (*c*) angular velocity.
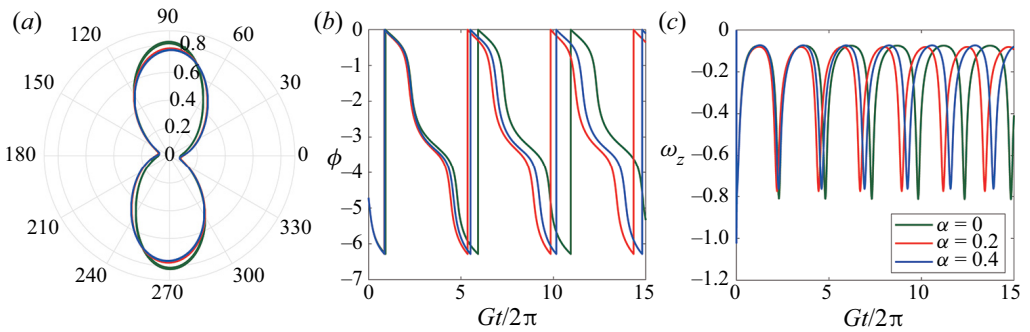

Figure 9. Effect of mobility parameter on particle rotation ($Wi = 2.0$, $AR = 2.0$): (*a*) angular velocity vs particle orientation; (*b*) azimuthal angle; (*c*) angular velocity.

is almost the same. Unlike the solvent viscosity ratio, the particle rotation period is a non-monotonic function of the mobility factor. The mobility factor affects viscoelastic flows in two main regards (Li *et al.* 2015): (i) reducing the elastic stress; and (ii) strengthening the fluid inertial effect through decreasing the apparent viscosity of fluids. Compared with the viscoelastic shear flow with $\alpha = 0.0$ (Oldroyd-B fluid), the elastic stress is weaker in the flows with $\alpha > 0.0$, and thus the particle rotates faster. For example, when $\alpha = 0.2$, the particle rotation period is less than that in an Oldroyd-B fluid. However, when $\alpha = 0.4$, the particle rotation slows down again. This non-monotonic relationship between the particle rotation period and the mobility factor is related to the shear-thinning and extension-hardening rheology of viscoelastic fluids. The role of the shear-thinning rheology in the particle rotation can be explained by the effect of fluid inertia, which has been studied systematically in Newtonian shear flows (Mao & Alexeev 2014).

On the other hand, the extension-hardening rheology of viscoelastic fluids is suppressed by increasing the mobility factor (Giesekus 1982). Moreover, Debbaut & Crochet (1988) indicated that the extension-hardening effect could increase the drag on the sphere in viscoelastic fluids. In the present flow system, compared with the case of $\alpha = 0.2$, the extension-hardening effect in the flow with $\alpha = 0.4$ is weaker, and thus the hydrodynamic torque exerted on the particle is decreased due to the attenuated drag force of the particle. Therefore, the particle rotation period is enlarged with $\alpha = 0.4$. The above results indicate that there exists a critical α to minimize the reduction of the particle rotation rate in viscoelastic shear flows.

3.2. *Three-dimensional rotation modes of particle in viscoelastic–inertial shear flow*

The 3-D rotation and orientation modes of particles have been extensively studied in Newtonian shear flows (Mao & Alexeev 2014; Rosén *et al.* 2014, 2015*a*) or viscoelastic shear flows neglecting fluid inertia (Stokes flow) (D'Avino *et al.* 2014). However, the coupled effect of fluid inertia and viscoelasticity on the rotation modes of particles has not been explored. Therefore, in this section, the rotation modes of a prolate particle ($AR = 4.0$) in the viscoelastic shear flow at $Re_p = 10.0$ are studied numerically. The mobility factor α and the solvent viscosity ratio β are set as $\alpha = 0.2$ and $\beta = 0.0909$, respectively.

3.2.1. *Tumbling mode with weak fluid elasticity*

Firstly, we analyse the particle rotation modes in viscoelastic shear flows with weak fluid elasticity. The tumbling mode of the prolate particle is shown in figure 10 and we find that, when fluid elasticity is weak, the particle spirals out to the shear plane and eventually tumbles around the vorticity direction. This particle rotation mode is similar to that in Newtonian shear flow with the same fluid inertial effect ($Re_p = 10.0$). According to the analysis by Rosén *et al.* (2014, 2015*a*), particle inertia induces the tumbling mode in the shear plane. Thus, the present tumbling mode of the particle in weakly viscoelastic shear flow is also caused by particle inertia.

In addition, the particle orbit drift is also modified by fluid elasticity. The particle orbit drift can be quantified by the orbit parameter C_b and the orbit drift rate c'. These two parameters have been widely used to analyse the particle orbit drift in Newtonian shear flows (Lundell & Carlsson 2010; Mao & Alexeev 2014; Rosén *et al.* 2014). The normalized orbit parameter C_b is formulated as follows (Mao & Alexeev 2014):

$$C_b = \frac{C}{C+1}, \tag{3.2}$$

$$C = AR^{-1} \tan\theta \sqrt{\left(AR^2 \sin^2\phi + \cos^2\phi\right)}, \tag{3.3}$$

where θ and ϕ are the polar angle and azimuthal angle of the particle symmetry axis, respectively.

The rate of orbit drift is quantified by the parameter c', defined as (Lundell & Carlsson 2010)

$$c' = \frac{2 \ln\left(C_{\phi=-\pi/2}/C_{\phi=-3\pi/2}\right)}{T_J}, \tag{3.4}$$

where T_J is the period of the Jeffery orbit (Jeffery 1922). Herein, the above two orbit parameters are also utilized to evaluate the effect of fluid elasticity on the particle orbit drift, as shown in figure 11.

Figure 11(*a*) shows the evolution of the particle orbit parameter C_b. Compared with the Newtonian case ($El = 0$), the time required for a particle to drift to the shear plane ($C_b = 1.0$) is obviously increased. This means that fluid elasticity slows down the particle drift process. The reason is that the drift direction of the particle orbit induced by weak fluid elasticity is opposite to that driven by particle inertia: weak fluid elasticity drives the particle to the vorticity direction, while particle inertia makes the particle spiral out to the shear plane (seen in figure 10). Therefore, fluid elasticity would weaken the effect of particle inertia on the particle orbit drift. In figure 11, the particle inertia is still dominant in viscoelastic shear flow due to the weak fluid elasticity, and thus the particle finally tumbles
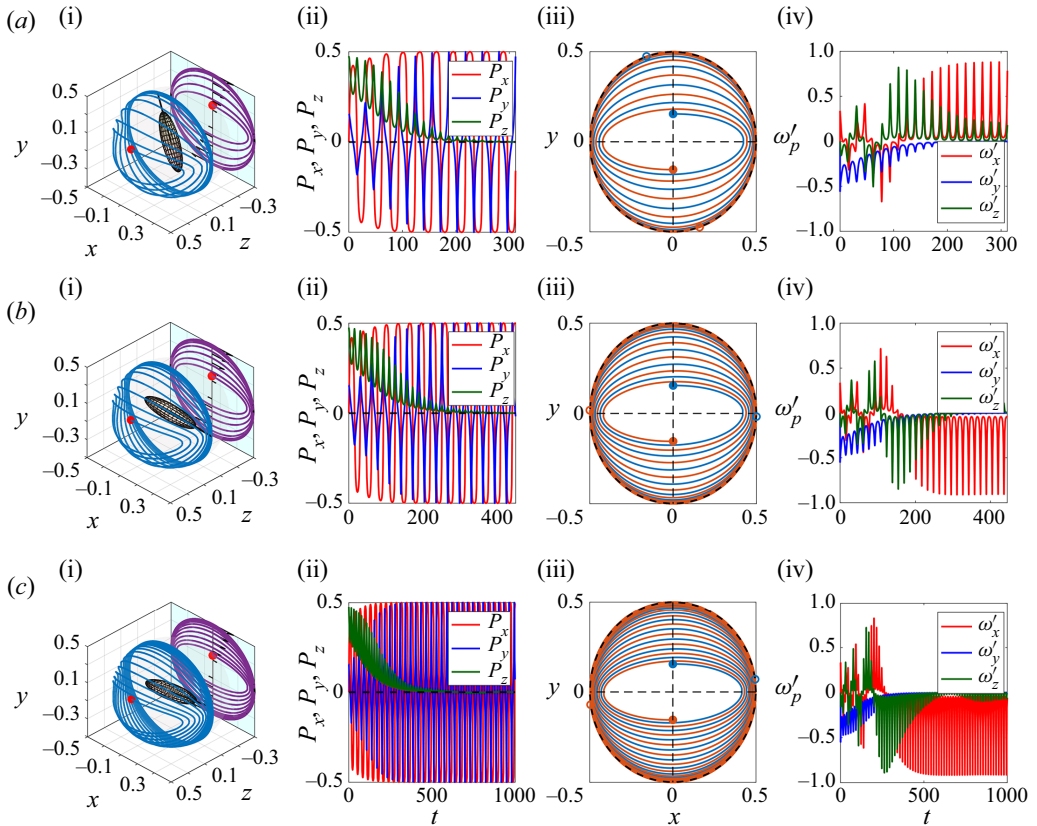
Figure 10. Tumbling mode of particle in viscoelastic shear flows with weak fluid elasticity: (*a*) $El = 0$; (*b*) $El = 0.005$; (*c*) $El = 0.01$. Panels (*a* i–*c* i) show the 3-D trajectory of particle tip; (*a* ii–*c* ii) show the coordinates of particle symmetry axis; (*a* iii–*c* iii) show the projection of 3-D trajectory of particle tip on the shear plane (*x*–*y* plane); (*a* iv–*c* iv) show the particle angular velocities ($\omega'_{p=x,y,z}$) in the particle frame. The filled and open circles in (*a* i–*a* iii) and (*c* i–*c* iii) denote the initial and final positions of the particle, respectively.
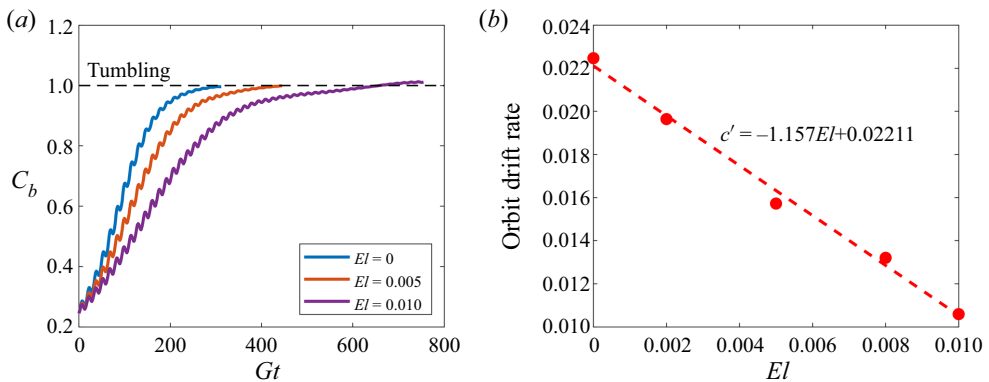
Figure 11. Effect of weak fluid elasticity on the particle orbit drift: (*a*) orbit parameter; (*b*) orbit drift rate. The initial particle orientation is $(\phi, \theta, \psi)_0 = (0.5\pi, 0.1\pi, 0)$ and $Re_p = 10.0$. Red dashed line in (*b*) is a fitting curve.
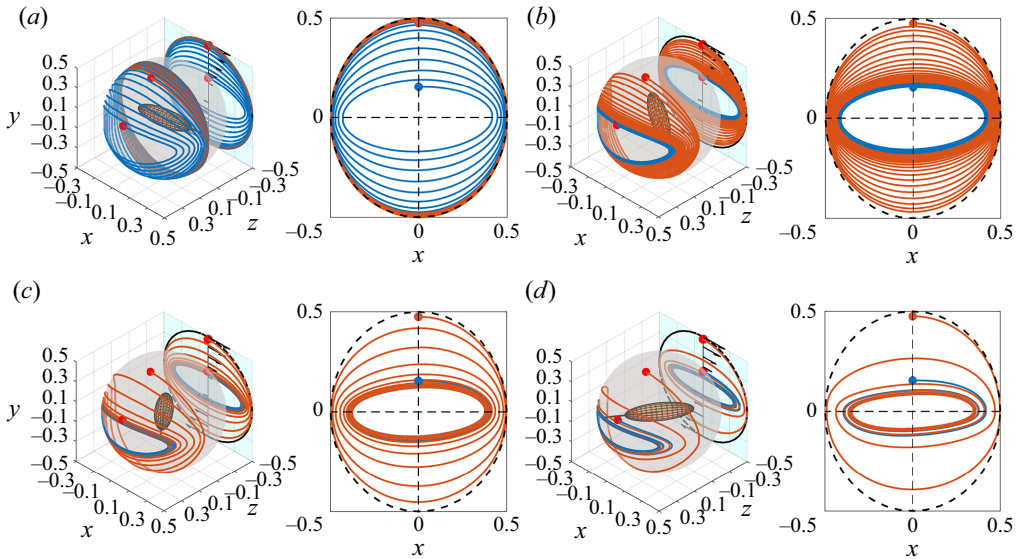
Figure 12. Trajectory of particle tip in viscoelastic flows with different elastic numbers: (*a*) $El = 0.01$; (*b*) $El = 0.03$; (*c*) $El = 0.05$; (*d*) $El = 0.1$. Different colours denote different initial particle orientations.

in the shear plane. From figure 11(*a*), it is found that the particle orbit parameter C_b varies nonlinearly with time, which is similar to that in the Newtonian case. Specifically, the closer the particle is to the shear plane, the more slowly the particle orbit drifts.

To further quantitatively describe the effect of fluid elasticity on the drift rate of the particle orbit, figure 11(*b*) shows the relation between the particle orbit drift rate and the elastic number, *El*. In figure 11(*b*), the orbit drift rate is negatively correlated with *El*, indicating fluid elasticity attenuates the particle orbit drift rate. The fitting curve in figure 11(*b*) reveals that the particle orbit drift rate is approximately linearly correlated with the elastic number within the ranges of *El* considered in the present study.

3.2.2. *Asymmetric-kayaking mode with moderate fluid elasticity*

In this section, we focus on the particle rotation behaviour in viscoelastic shear flows with moderate fluid elasticity. In this situation, the final rotation mode of the particle is determined by the competition among the fluid inertia, particle inertia and fluid elasticity.

Figure 12 shows the 3-D trajectories of the particle tip at two different initial orientations, i.e. $(\phi, \theta, \psi)_0 = (0.5\pi, 0.4\pi, 0)$ and $(0.5\pi, 0.1\pi, 0)$. As a contrast, the particle rotation mode induced by weak fluid elasticity ($El = 0.01$) is also included in figure 12(*a*). The comparisons between figures 12(*a*) and 12(*b–d*) reveal that, with increasing fluid elasticity, the drift direction of particle orbit is changed: the particle spirals toward a specific closed orbit between the vorticity axis and shear plane, and finally rotates along a Jeffery-like orbit, which depends upon the fluid elasticity. This peculiar rotation mode, caused by the interplay between fluid elasticity and inertial effects, is similar to the kayaking mode (Rosén *et al.* 2014) in Newtonian shear flows.

To quantify the modulations of particle orbit drift by moderate fluid elasticity, figure 13 shows the evolution of the particle orbit parameter C_b under moderate fluid elasticity ($El = 0.03 \sim 0.1$). Here, we find that the actual drift direction of the particle orbit is determined by the relative position of the particle initial orientation to the final equilibrium orbit. The particle always migrates to the equilibrium orbit despite different initial orientations.
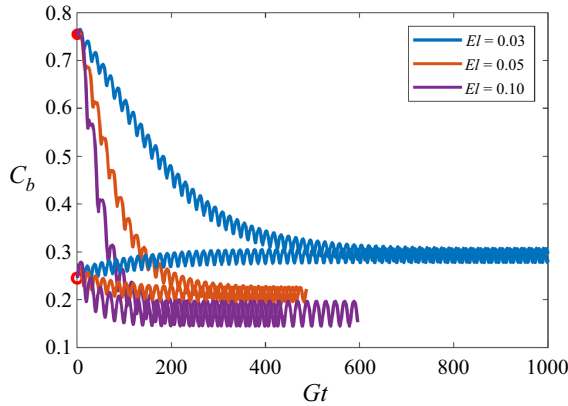
Figure 13. Evolution of particle orbit parameter in viscoelastic shear flow with moderate fluid elasticity. The red filled and open circles at $t = 0$ denote two different initial orientations.

This observation indicates that this final equilibrium orbit is a stable limit cycle in phase space. In the Newtonian case, there exists an unstable limit cycle between the shear plane and vorticity direction (Rosén *et al.* 2014). Figure 13 also shows that the particle orbit parameter is a nonlinear function of time. The drift rate of the particle orbit slows down when the particle approaches the final equilibrium orbit. Different from the case with weak fluid elasticity (figure 11), the moderate fluid elasticity accelerates the drifting process of the particle orbit. This means that the particle can be quickly attracted to the equilibrium orbit through increasing fluid elasticity.

Figure 14 shows the final equilibrium orbits of particles at different elastic numbers, *El*. As shown in figure 12, in viscoelastic shear flows with moderate fluid elasticity, the particle eventually rotates along a Jeffery-like orbit periodically. However, the shape of the present equilibrium orbit is different from the Jeffery orbit (Jeffery 1922) in Newtonian flows, the projection of Jeffery orbits on the shear plane is axisymmetric to the *x* or *y* axis (the green circle in figure 14), while the projection of the present equilibrium orbit is asymmetric about the *x* or *y* axis. Therefore, referring to the kayaking rotation mode of the particle in Newtonian shear flows, the present rotation mode associated with the asymmetric equilibrium orbit could be named the asymmetric-kayaking mode. Figure 14 also reveals that, with increasing fluid elasticity, the deviation between the present equilibrium orbit and the Jeffery orbit is more obvious. Thus, the asymmetry of the equilibrium orbit is more remarkable.

Moreover, the sensitivities of the tumbling and asymmetric-kayaking modes to the rheological parameters (α and β) of viscoelastic fluids are demonstrated in figures 15 and 16. In figure 15(a), it is found that, in weakly viscoelastic flows with different mobility factors $\alpha = 0.0, 0.2$ and 0.4, the spheroid finally shows the tumbling mode in the shear plane, and the orbit drift rates are almost unchanged by α. Similarly to the mode observed in figure 14(c), when the fluid inertia and fluid elasticity are comparable, particle rotation remains in the asymmetric-kayaking mode in viscoelastic shear flows with different α. However, the final equilibrium orbit of the spheroid is determined by α: the larger α is, the flatter the shape of the steady orbit (figure 15c).

Figure 16 shows the effect of the solvent viscosity ratio ($\beta = 0.0454, 0.0909$ and 0.1818) on the spheroid rotation modes. Similarly to the mobility factor, the rotation modes of the spheroid are slightly affected by the solvent viscosity ratio. The prolate spheroid eventually shows the tumbling mode and asymmetric-kayaking mode when $El = 0.005$ and
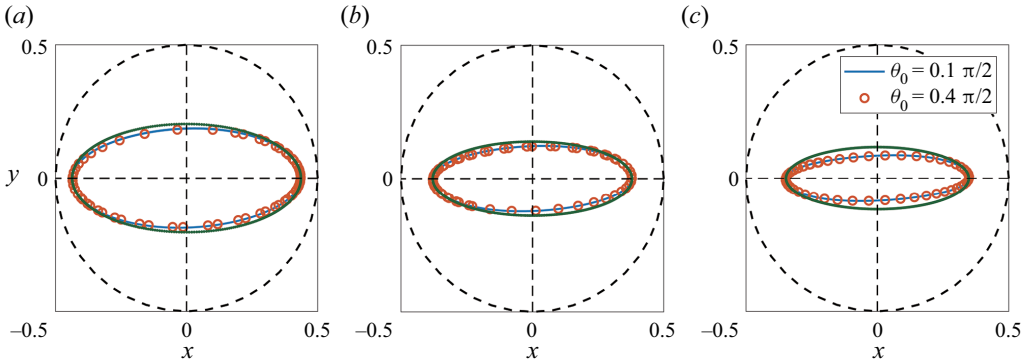
958 A20-18

Figure 14. Steady asymmetric-kayaking mode in viscoelastic flows with different elastic numbers: (*a*) $El = 0.03$; (*b*) $El = 0.05$; (*c*) $El = 0.1$. The green line is the Jeffery orbit (Jeffery 1922).
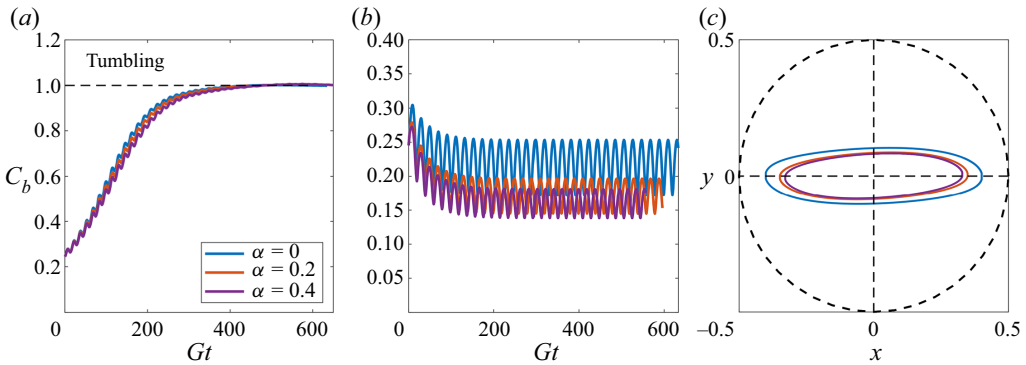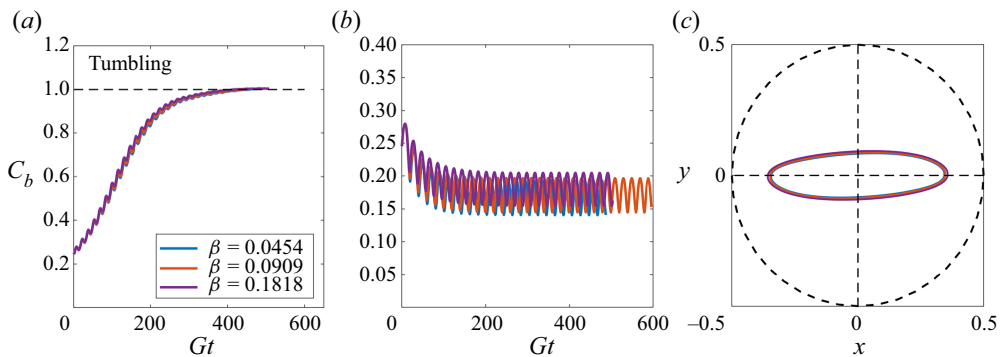

Figure 15. Effect of mobility factor on the rotation modes of spheroid in shear flow with weak ($El = 0.005$) and moderate ($El = 0.1$) fluid elasticities, $AR = 4.0$, $Re_p = 10.0$, $\beta = 0.0909$: orbit parameter at $El = 0.005$ (*a*) and $El = 0.1$ (*b*); (*c*) equilibrium asymmetric-kayaking mode at $El = 0.1$.

Figure 16. Effect of solvent viscosity ratio on the rotation modes of spheroid in shear flow with weak ($El = 0.005$) and moderate ($El = 0.1$) fluid elasticities, $AR = 4.0$, $Re_p = 10.0$, $\alpha = 0.2$: orbit parameter at $El = 0.005$ (*a*) and $El = 0.1$ (*b*); (*c*) equilibrium asymmetric-kayaking mode at $El = 0.1$.
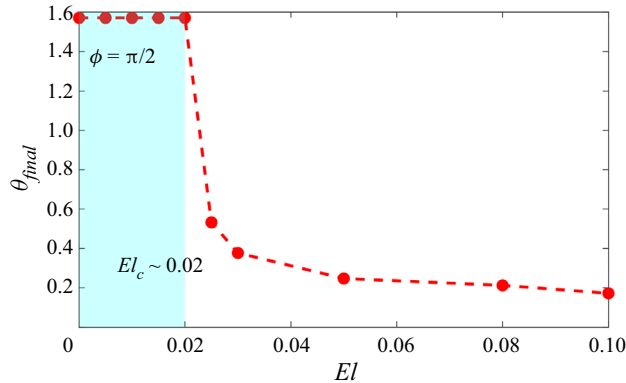
Figure 17. Polar angle of the intersection point of the equilibrium orbit and y axis ($\phi = \pi/2$).

$El = 0.1$, respectively. Within the present range of α and β, compared with the solvent viscosity ratio, the rotation modes are more sensitive to the mobility factor.

Finally, from results in § 3.2.1 (weak fluid elasticity) and § 3.2.2 (moderate fluid elasticity), we conclude that there exists a critical elastic number, El_c, governing the transitions of particle rotation modes in viscoelastic shear flows with $Re_p = 10.0$: (i) when $El < El_c$, the particle inertia is dominant and the particle exhibits the 'tumbling mode' in the shear plane; (ii) with $El > El_c$, the fluid elasticity and inertial effects become comparable, the competition makes particle rotate in the 'symmetric-kayaking mode'. In the present simulation, this critical elastic number is estimated numerically as $El_c \sim 0.02$, as shown in figure 17. This means that, with the present simulation parameters, once the elastic number exceeds 0.02, the final particle rotation mode begins to be primarily affected by fluid elasticity. Note that the present El_c is of the same order as the critical elastic number governing the elasto-inertial lateral migration of spherical particles ($El_c \sim 0.01$) (Li *et al.* 2015). This further indicates that when the elastic number in viscoelastic flow systems reaches $O(0.01)$, the effect of fluid elasticity on both the migration and rotation of particles has to be considered.

3.2.3. *Rotation modes induced by strong fluid elasticity*

In this section, we examine the particle rotation modes in viscoelastic shear flows with strong fluid elasticity. As shown in figure 18, we find that, with increasing fluid elasticity, the particle shows a rolling mode between the flow and vorticity directions, a bi-stable orientation mode and a flow-alignment mode. Except for $El = 0.4$ (figure 18b), the final orientations of the particle released from different initial positions are consistent (figure 18a,c), which indicates that the rolling mode in the flow–vorticity plane (figure 18a) and the flow-alignment mode (figure 18c) are both stable (stable fixed point in phase space). Interestingly, the bi-stable orientation mode reported in the experiments (Johnson *et al.* 1990; Gunes *et al.* 2008) and numerical simulations in viscoelastic shear flow with zero fluid inertia (D'Avino *et al.* 2014) is also found in the present viscoelastic shear flow with finite fluid inertia. Overall, the particle orientation modes under the present flow conditions are similar to those in viscoelastic shear flows without fluid and particle inertia. This indicates that, once fluid elasticity becomes fully dominant in a flow system, the particle rotational dynamics in viscoelastic–inertial shear flows could still be predicted by the results obtained with the Stokesian flow assumption.
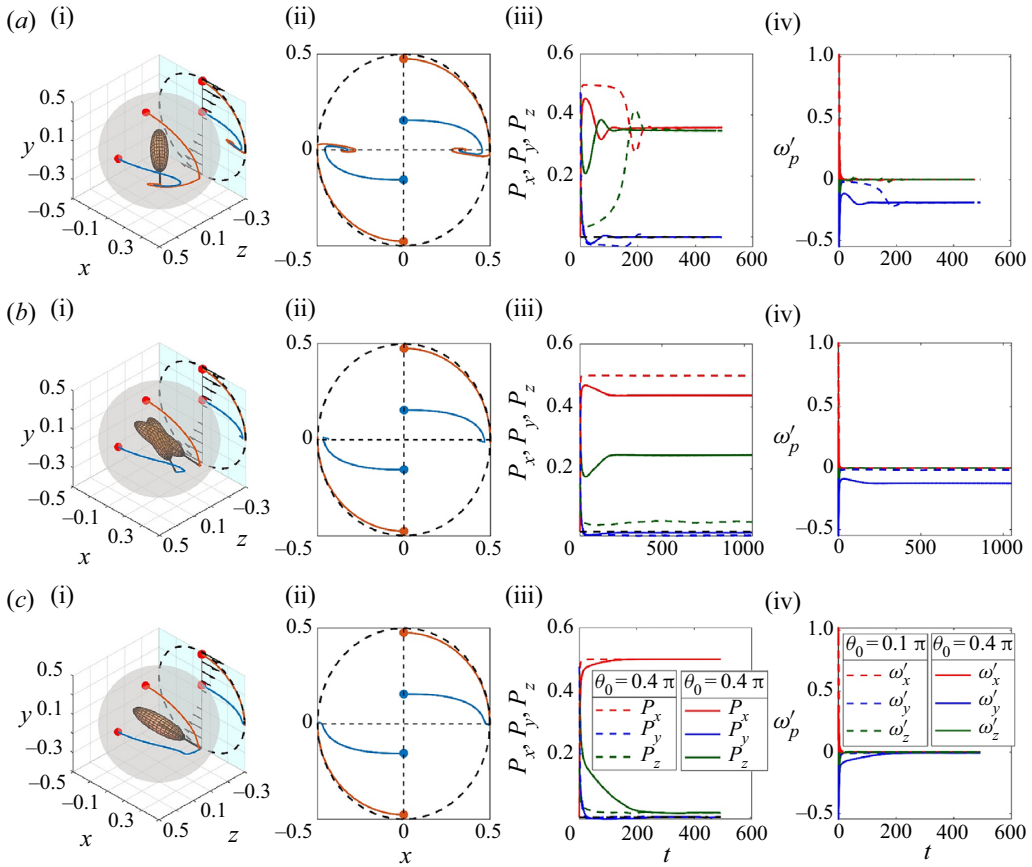
Figure 18. Particle rotation modes induced by the strong fluid elasticity: (*a*) $El = 0.3$; (*b*) $El = 0.4$; (*c*) $El = 0.5$. The different colours of particle trajectories in (*a* i–*c* i) and (*a* ii–*c* ii) denote particles released from different initial orientations $(\phi, \theta, \psi)_0 = (0.5\pi, 0.4\pi, 0)$ and $(0.5\pi, 0.1\pi, 0)$, respectively. The solid and dashed lines in (*a* iii–*c* iii) and (*a* iv–*c* iv) represent the coordinates and angular velocities $(\omega'_{p=x,y,z})$ of the particles with the above two different initial orientations.

When the fluid elasticity becomes dominant in the flow system, the rheological properties of viscoelastic fluids are highly dependent on α and β. Both figures 19 and 20 reveal that α and β significantly affect the particle orientation modes in the shear flow with strong fluid elasticity. As shown in figure 19, with increasing α, the fluid elasticity is suppressed, thus the equilibrium orientation of the particle is approaching the vorticity direction (figure 19*b*,*c*). When α increases to $\alpha = 0.4$, the attenuated fluid elasticity is not dominant in the flow system, then the comparable fluid inertia and fluid elasticity together induce the asymmetric-kayaking mode, which is similar to the rotation mode observed in the shear flow with the moderate fluid elasticity (figure 12).

Figure 20 shows the dependence of the orientation modes of the prolate spheroid on the solvent viscosity ratio. As discussed in § 3.1, the smaller the solvent viscosity ratio is, the stronger the fluid elastic stress is. From this point of view, as β varies from $\beta = 0.0454$ to $\beta = 0.1818$, the fluid elasticity attenuates in the flow system, thus the prolate particle finally exhibits the flow-alignment state (figure 20*a*), the inclined-rolling mode between the flow and vorticity directions (figure 20*b*) and the asymmetric-kayaking mode (figure 20*c*). It is worthwhile noting that, although these two rheological parameters can
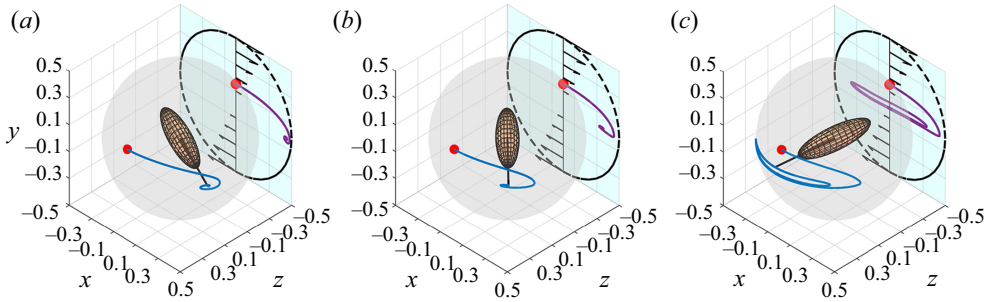
958 A20-21

Figure 19. Effect of mobility factor on the orientation modes of prolate spheroid in the shear flow with strong ($El = 0.3$) fluid elasticity, $AR = 4.0$, $Re_p = 10.0$, $\beta = 0.0909$. (a) $\alpha = 0$, (b) $\alpha = 0.2$, (c) $\alpha = 0.4$.
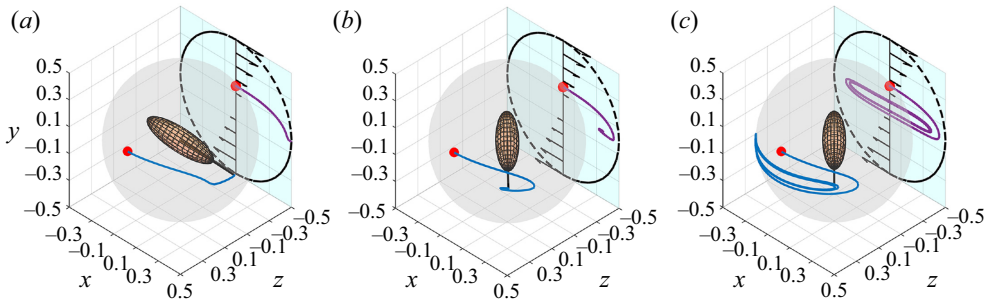

Figure 20. Effect of solvent viscosity ratio on the orientation modes of a prolate spheroid in the shear flow with strong ($El = 0.3$) fluid elasticity, $AR = 4.0$, $Re_p = 10.0$, $\alpha = 0.2$. (a) $\beta = 0.0454$, (b) $\beta = 0.0909$, (c) $\beta = 0.1818$.

modulate the critical elastic number El_c, which governs the transition of particle rotation modes, the mechanism behind the transitions of particle rotation modes is consistent with that discussed in previous sections.

On the other hand, the fluid inertia can also modulate the particle rotation modes in the viscoelastic shear flow with strong fluid elasticity. Figure 21 shows that, with increasing fluid inertia (Re_p), the particle gradually approaches the shear plane. When $Re_p < 8.0$, the fluid elasticity is dominant in the flow system, and thus the particle orientation modes are similar to those in the viscoelastic flow with negligible fluid inertia ($Re_p = 0.1$). However, the angle between the particle symmetry axis and the shear plane is changed due to the fluid inertia (figure 21a–c). When the fluid inertia becomes more dominant ($Re_p > 13.0$), the particle is driven to the shear plane and finally reaches a steady state, which is similar to the rotation mode of the particle in a Newtonian shear flow with large fluid inertia ($Re_p \sim 100.0$) (Rosén *et al.* 2014). The steady angle between the particle symmetry axis and flow direction is slightly modulated by the higher $Re_p = 40.0$ and $Re_p = 50.0$. Note that, different from the Newtonian case, such a motionless state of a particle in the shear plane within the present elasto-inertial shear flow can be realized with moderate fluid inertia ($Re_p \sim 13.0$). This implies that it is convenient to manipulate the orientations of non-spherical particles in elasto-inertial flows with moderate fluid inertia, which corresponds to a small pressure gradient (less energy) used to operate microfluidic devices.
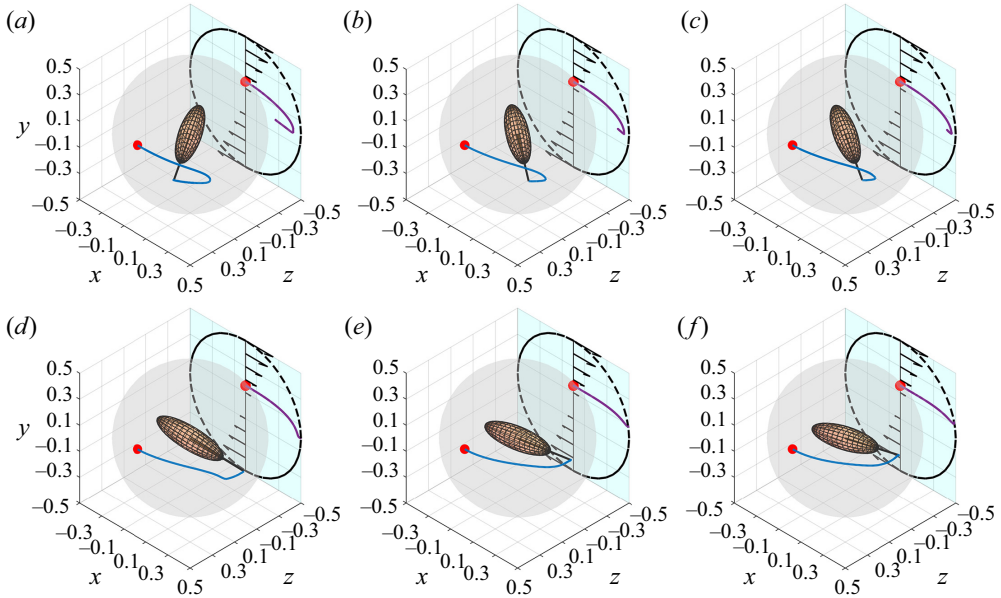
958 A20-22

Figure 21. Effect of fluid inertia on the orientation modes of a prolate spheroid with $AR = 4.0$, $El = 0.4$. The initial orientation of particle is $(\phi, \theta, \psi)_0 = (0.5\pi, 0.4\pi, 0)$. (a) $Re_p = 0.1$, (b) $Re_p = 5.0$, (c) $Re_p = 8.0$, (d) $Re_p = 13.0$, (e) $Re_p = 40.0$, (f) $Re_p = 50.0$.
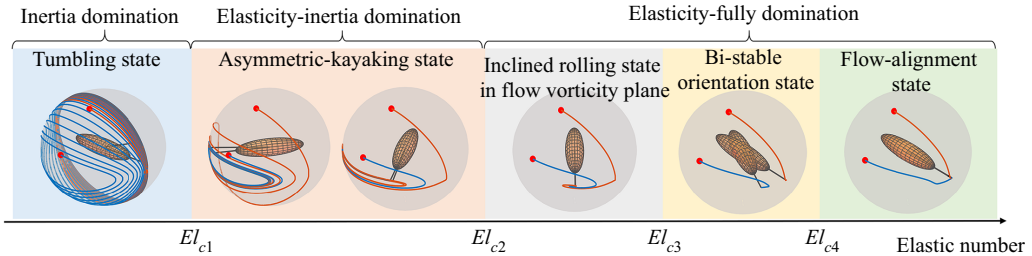

Figure 22. Illustration of multi-orientation modes of a neutrally buoyant prolate particle ($AR = 4.0$) in viscoelastic shear flow with finite fluid inertia ($Re_p = 10.0$). Here, $El_{c1\sim c4}$ are four critical elastic numbers that classify particle rotation modes.

Finally, according to results in §3.2, an overall picture of rotation modes for a neutrally buoyant prolate particle in viscoelastic–inertial shear flows is plotted in figure 22. Compared with the observed particle orientation modes in viscoelastic shear flows with zero fluid and particle inertia (D'Avino *et al.* 2014), the rotational and orientational dynamics of neutrally buoyant particles in the present viscoelastic shear flows is more complicated. Figure 22 shows four critical elastic numbers that classify particle rotation modes. In contrast to the earlier studies on the viscoelastic shear flow system within the Stokesian regime, there are two additional critical elastic numbers given in the present flow system. Consequently, a newly observed rotation mode (asymmetric-kayaking mode) induced by the competition among the fluid elasticity, fluid inertia and particle inertia, occurs in the present particle-laden viscoelastic flow system with finite fluid inertia ($Re_p = 10.0$).

In a summary, figure 22 clearly reveals that the neutrally buoyant non-spherical particles exhibit multi-rotation modes in viscoelastic–inertial shear flows. These peculiar orientational characteristics have not been found in the flow systems governed by a single effect. The present results could be potentially used to design the rheology-based control strategy for guiding particles to realize specific orientations in complex fluids.

4. Conclusions

In this work, we numerically investigate the rotational and orientational dynamics of a neutrally buoyant spheroid immersed in viscoelastic shear flow with finite fluid inertia. The fluid viscoelasticity is described by the Giesekus model. The interplay between particle and viscoelastic fluid is realized by the IBM. With weak fluid inertia ($Re_p = 0.1$), the influence of fluid rheology on the particle rotational dynamics in the shear plane is analysed in detail. For moderate fluid inertia ($Re_p = 10.0$), we focus on the modulations of the particle 3-D orbit for different fluid elasticities. The main conclusions are:

(i) With weak fluid inertia, the particle rotation rate is remarkably reduced by fluid elasticity. The particles with large eccentricity ($AR = 4.0$) reach a non-rotational state in viscoelastic shear flow ($Wi = 2.0$). This observation reveals that, within the range of Wi considered in the present study ($Wi = 0.0 \sim 5.0$), fluid elasticity stabilizes the particle rotation in a viscoelastic fluid. Additionally, the fluid elasticity brings asymmetry into the particle rotation process where the particle deceleration takes a longer time than acceleration.

(ii) The rotational dynamics of particles are affected by the solvent viscosity ratio and the mobility factor in different ways: the period of the particle rotation decreases monotonically with the solvent viscosity ratio. In contrast, the particle rotation period changes non-monotonically with the mobility factor. The results indicate that there exists a critical mobility factor for a viscoelastic fluid to minimize the reduction of the particle rotation rate in viscoelastic shear flows.

(iii) With moderate fluid inertia, when fluid elasticity is weak, the particle spirals toward the shear plane and eventually exhibits a tumbling mode, which is caused by the particle inertia. The fluid elasticity slows down the drift rate of the particle orbit. With increasing fluid elasticity, the competition among fluid elasticity, fluid inertia and particle inertia cause the particle to be attracted to a stable limit cycle between the shear plane and vorticity direction. This stable limit cycle results in a new particle rotation mode, i.e. asymmetric-kayaking mode.

(iv) The neutrally buoyant prolate particles exhibit multi-rotation modes in viscoelastic–inertial shear flows. Compared with the orientation behaviour of inertia-free particles in the Stokesian viscoelastic shear flows, four critical elastic numbers and one new orientation mode (asymmetric-kayaking mode) are observed in the present particle-laden viscoelastic flow system with finite fluid inertia.

In summary, the main contributions of the present work are: (i) comprehensively elaborating on the effects of rheological factors of viscoelastic fluid on the particle rotational dynamics; and (ii) a first attempt to give the overall picture of rotation modes induced by the elasto-inertial effect for a neutrally buoyant spheroid in viscoelastic shear flow at a finite Reynolds number. The results of the present work might enrich our understanding of the peculiar rotation and orientation dynamics of non-spherical particles in viscoelastic–inertial flows. Furthermore, from the applied perspective, the present

results could also potentially be used to design a rheology-based controlling strategy for guiding particles to realize specific orientations in complex fluids.

Finally, it is worthwhile noting that the present computational framework of particle-laden viscoelastic flow is convenient to tackle the rotation of complex particles. A possible extension of the present research is to explore the elasto-inertial rotation of spheroids with a non-smooth or non-analytical closed surface, which may give additional insights into the dynamics of complex particles in viscoelastic fluids.

Declaration of interests. The authors report no conflict of interest.

Author ORCIDs.
- Yansong Li https://orcid.org/0000-0001-7506-5384;
- Chunxiao Xu https://orcid.org/0000-0001-5292-8052;
- Lihao Zhao https://orcid.org/0000-0002-3642-3051.

Appendix A. Validation of numerical approach

The present study aims at investigating the rotation of particles in viscoelastic shear flows. Thus, we validate the numerical methods from two aspects: (i) particle rotation and (ii) fluid elastic effect.

A.1. *Spheroid rotation in a Newtonian shear flow with zero fluid inertia*

Jeffery orbit (Jeffery 1922) is a canonical benchmark problem used to check the accuracy of a particle solver (Rosén *et al.* 2014, 2015*a*). We used it here to validate the performance of the present particle solver when resolving the particle rotational dynamics. In this validation case, the particle aspect ratio is set as $AR = 2.0$, and the particle Reynolds number and Stokes number are consistent, i.e. $Re_p = St = 0.1$. Thus, both the fluid and particle inertial effects are weak. The comparisons of numerical and theoretical results (Jeffery 1922) are shown in figure 23, in which the calculated particle orientation and angular velocity agree well with the theoretical results. The comparison of results indicates that the present numerical method could accurately predict particle rotation in linear shear flow.

A.2. *Spheroid rotation in a viscoelastic shear flow with zero fluid inertia*

The particle rotation in the viscoelastic shear flow within the Stokesian regime is used to check the capability of the present method to capture the fluid elastic effect on particle rotation. In this test case, the particle Reynolds number is $Re_p = 0.1$. The Weissenberg number ranges from 0 to 4.0. We first validate the dependence of average angular velocity, $\bar{\omega}$, of particles with different aspect ratios on the Weissenberg number. The comparison of results is shown in figure 24, in which the calculated average angular velocity of particles is generally consistent with the reference results from D'Avino *et al.* (2014), although a little deviation exists when the fluid elastic effect becomes significant ($Wi > 1.0$). Such little deviation might be caused by two reasons: (i) the momentum equation used is different, in the present study, the Navier–Stokes equation is utilized to resolve the flow field, while the Stokes equation is used in the reference; (ii) the solution method of the constitutive equation is different. In the present study, the constitutive equation is solved by the standard-conformation tensor formulation, whereas the log-representation formula
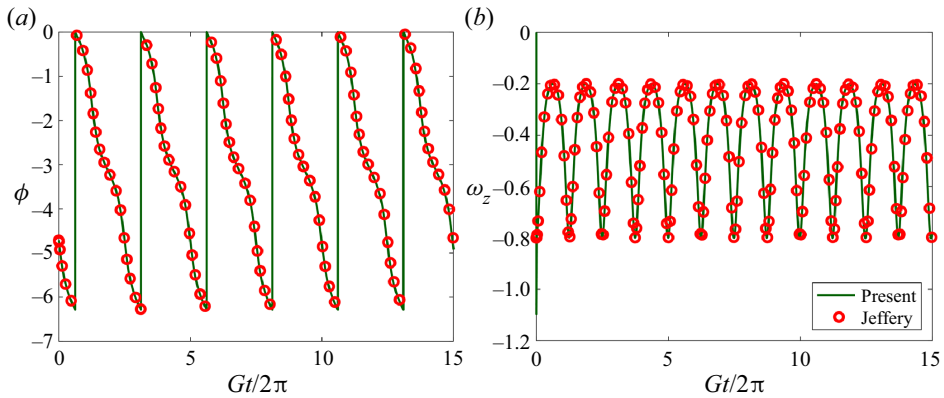
Figure 23. Comparisons of calculated results of a prolate spheroid ($AR = 2.0$) with theoretical solutions of Jeffery (1922): (*a*) azimuthal angle; (*b*) angle velocity.
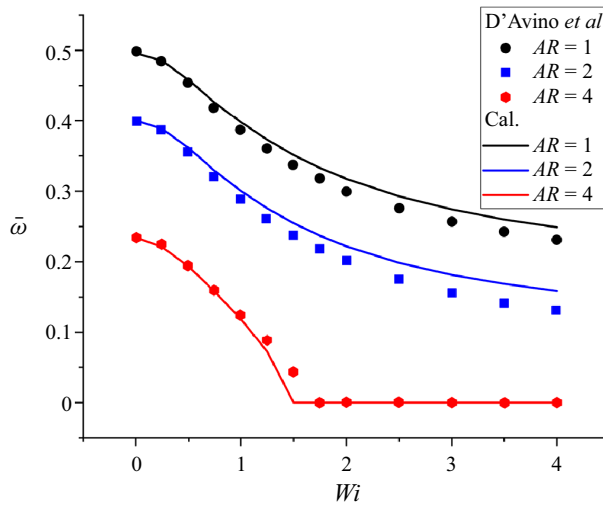

Figure 24. Comparisons of calculated average angular velocity of particle with the results from D'Avino *et al.* (2014).

is used by D'Avino *et al.* (2014) to stabilize the simulation of viscoelastic flow with strong fluid elasticity. There may be a little difference in resolving the viscoelastic fluid–solid interaction by these two methods under the highly elastic effect (Castillo & Codina 2015).

From figure 24, we can see that the rotational dynamics of the particle with large eccentricity is more easily affected by fluid elasticity. Specifically, the particles with large aspect ratios ($AR = 4.0$) can remain stationary in highly viscoelastic shear flow ($Wi > 1.5$). Overall, the comparison of results shows that the present numerical method could readily estimate the reduction of the particle rotation rate by fluid elasticity.

To further validate the performance of the present method for predicting the orientation of non-spherical particles in viscoelastic shear flows, we also contrast the particle orientation modes calculated with those from previous results (D'Avino *et al.* 2014). Figure 25 illustrates the orientation modes of a prolate particle ($AR = 4.0$) under different fluid elasticities. From figure 25, it is found that the present method can capture the
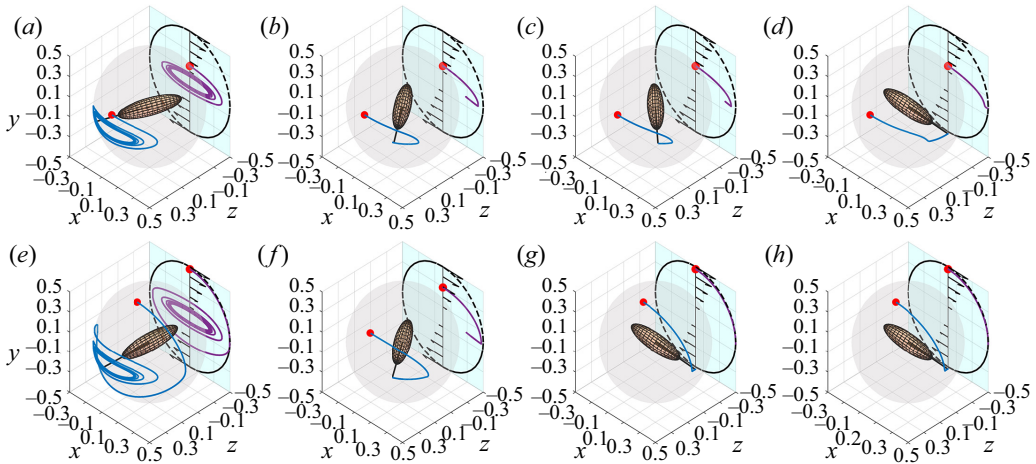
958 A20-26

Figure 25. Orientation modes of a neutrally prolate particle ($AR = 4.0$) in viscoelastic shear flows with different elasticities. (*a*) $Wi = 1.0$, (*b*) $Wi = 2.7$, (*c*) $Wi = 3.0$, (*d*) $Wi = 4.5$, (*e*) $Wi = 1.0$, (*f*) $Wi = 2.7$, (*g*) $Wi = 3.0$, (*h*) $Wi = 4.5$.

transitions of orientation modes of a prolate particle. There exist four different orientation modes in the present simulations: kayaking mode, orientation between the flow and vorticity direction, bi-stable orientation mode and flow-alignment mode. Different from the elasticity-induced orientation modes of inertia-free particles reported by D'Avino *et al.* (2014), the particle rotates as a 'kayaking' mode in the present simulation (figure 25*a*,*e*), rather than the 'log-rolling' mode in the weakly viscoelastic shear flows with zero inertial effect. However, the present 'kayaking' rotation mode is also found in the simulation by Wang *et al.* (2019).

The final rotational state of particles could reveal the dominant effect in the particle-laden flow system. If the final rotation mode is a time-periodic mode for particle and fluid flow, the dominant effect generally is particle inertia (Rosén *et al.* 2014). From this point, the particle inertia might result in the present kayaking mode in figures 25(*a*) and 25(*e*). Considering this, we additionally perform another case, where the particle density is less than that of the fluid, i.e. density ratio $\rho_r = 0.5$, to validate the effect of particle inertia on the present kayaking mode.

Figure 26 shows that, when decreasing particle inertia, the lighter particles with different initial orientations all spirally approach the vorticity direction, and finally behave in the 'log-rolling' mode as reported by D'Avino *et al.* (2014) for an inertia-free particle in weakly viscoelastic shear flows. Therefore, we might conclude that the present 'kayaking' mode might be due to particle inertia. Furthermore, the above test results indicate that the competition among fluid inertia (Re_p), particle inertia (St) and fluid elasticity (Wi) can lead to the peculiar particle rotation behaviours which could not be observed in the previous studies governed by a single effect. This motivates the present research in § 3.

A.3. *Spheroid rotation in a Newtonian shear flow with fluid inertia*

The present study focuses on the effect of fluid inertia on the rotational dynamics of spheroids in viscoelastic flows. Thus, we first examine the capability of the present numerical approach to capture the effect of fluid inertia on particle rotation in a Newtonian shear flow. In this test case, a spheroid with different aspect ratios ($AR = 2.0$ and 0.5)
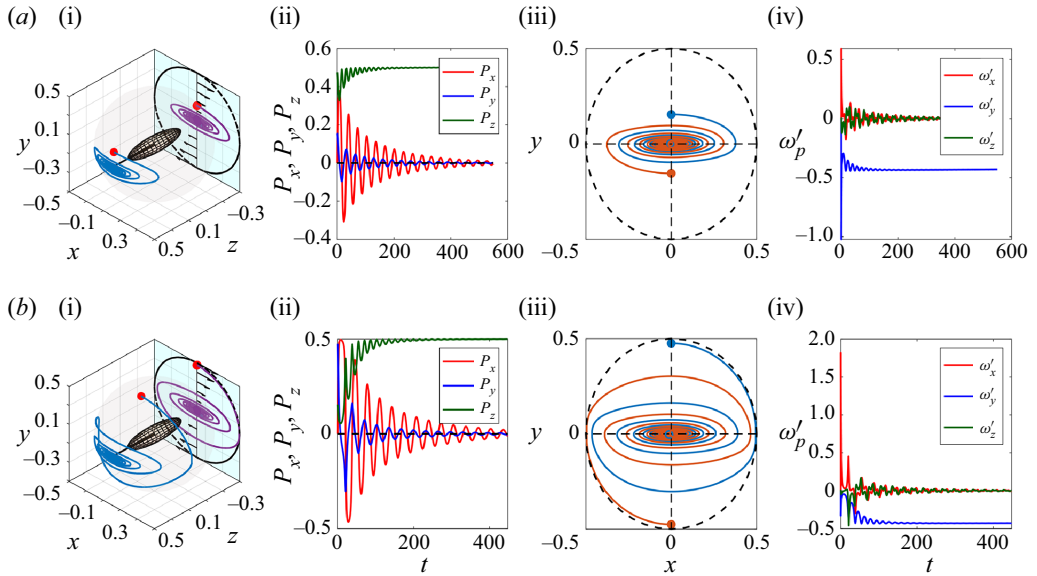
Figure 26. Effect of particle inertia on the orientation modes of a prolate particle ($AR = 4.0$) in viscoelastic shear flow with $Wi = 1.0$, $Re_p = 0.1$: panels (a i,b i) show the 3-D trajectory of the tip of particle with the different initial orientation $(\phi, \theta, \psi)_0 = (0.5\pi, 0.4\pi, 0)$ and $(0.5\pi, 0.1\pi, 0)$, respectively; (a ii,b ii) show the coordinates of the particle tip; (a iii,b iii) show the particle trajectory projected on the x–y plane; (a iv,b iv) show the particle angular velocities in the particle frame.
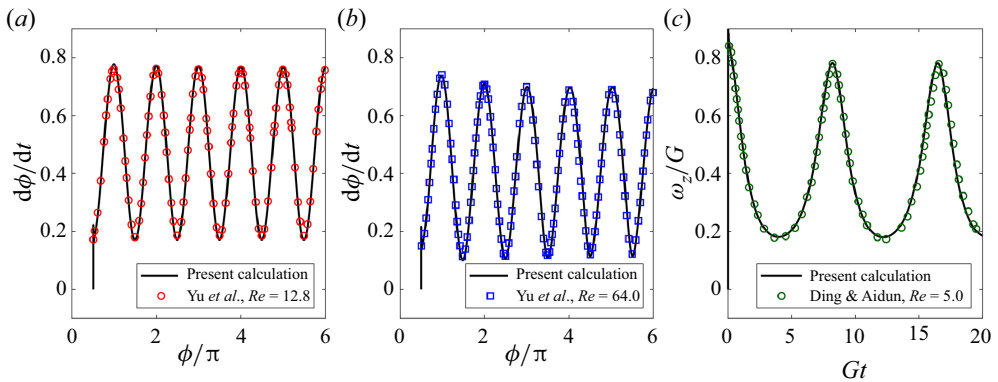

Figure 27. Comparison of calculated spheroid rotation rate with the reference results (Ding & Aidun 2000; Yu *et al.* 2007) in Newtonian shear flow with $AR = 2.0$ (a,b) and $AR = 0.5$ (c).

is immersed in a Newtonian shear flow at $Re_p = 5.0$, 12.8 and 64.0. The simulation parameters are consistent with those in earlier studies (Ding & Aidun 2000; Yu *et al.* 2007). The comparison of results is shown in figure 27, where the present spheroid rotation rate ($\mathrm{d}\phi/\mathrm{d}t$) at different azimuthal angles (ϕ) agrees well with that reported by Yu *et al.* (2007), as shown in figures 27(a) and 27(b). The angular velocity of the spheroid with $AR = 0.5$ is also in good agreement with that from Ding & Aidun (2000), as shown in figure 27(c). The comparison of results shows that the present numerical approach can capture the effect of fluid inertia on the spheroid rotation.
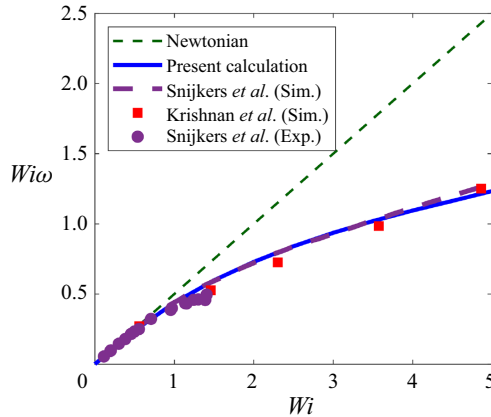
958 A20-28

Figure 28. Comparison of calculated spheroid rotation rate with the experiments (Snijkers *et al.* 2009) and simulation results (Snijkers *et al.* 2011; Krishnan, Shaqfeh & Iaccarino 2017).

A.4. *Sphere rotation in a sheared viscoelastic flow resolved within Navier-Stokes framework*

To explore the coupled effect of fluid elasticity and fluid inertia on particle rotation, we further verify the present numerical approach by computing the rotation of a single sphere immersed in a viscoelastic shear flow. The validation results are shown in figure 28, where the present angular velocity of the sphere agrees well with experiments (Snijkers *et al.* 2009) and with the numerical results obtained within the Navier–Stokes framework (Krishnan *et al.* 2017). This validation indicates that the present numerical methods within the Navier–Stokes framework are reliable in resolving the coupled effect of fluid elasticity and fluid inertia on particle rotation.

Moreover, the accuracy of the present numerical solver is systematically validated by several canonical benchmark examples of viscoelastic fluid flows in our recent study (Li *et al.* 2022).

In summary, the accuracy and capability of the present numerical approach are verified by four benchmark examples of particle rotation in Newtonian and viscoelastic shear flows. All validation results reveal that the present methods can accurately simulate the particle dynamics in viscoelastic shear flows.

A.5. *Grid resolution effect*

To check the effect of grid resolution on the particle rotation, we simulated the rotation of a prolate particle ($AR = 2.0$) in a viscoelastic shear flow on three meshes with different spatial resolutions; the results are shown in figure 29. The angular velocities at different orientations calculated on different meshes agree well with each other (figure 29*a*). This agreement indicates that the present grid resolution ($\Delta = 1/32D_p$) is capable of giving the grid-independence solution of particle angular velocity at different orientations.

To further evaluate the grid resolution effect on the 3-D orientation mode of the particle, we also calculated the 3-D trajectory of the particle tip ($AR = 4.0$) in viscoelastic shear flow with finite fluid inertia ($Re_p = 10.0$, $Wi = 5.0$). Figure 29(*b*) shows that the equilibrium orientation modes of the particle are not changed with increasing grid resolution. Note that a small domain size of $L \times H \times W = 2 \times 2 \times 2$ is chosen in this test case to save the computational cost.
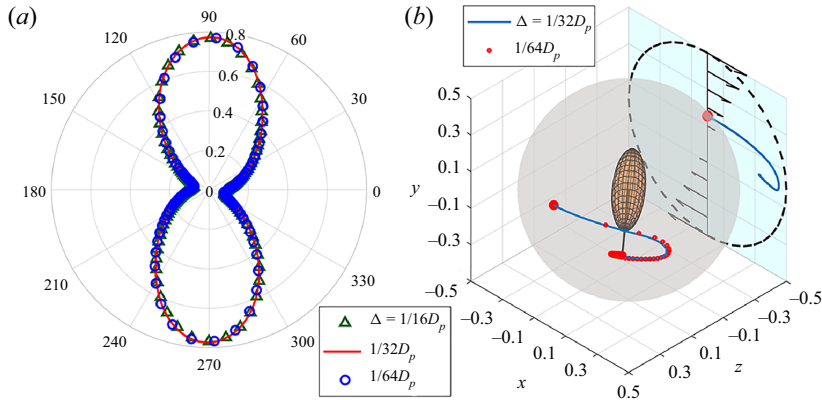
958 A20-29

Figure 29. Effect of grid resolution on the particle rotation: (*a*) angular velocity vs particle orientation in the polar coordinate system, $AR = 2.0, Re_p = 0.1, Wi = 2.0$; (*b*) orientation modes of a prolate spheroid with $AR = 4.0, Re_p = 10.0, Wi = 5.0$.

Moreover, in earlier studies on the single effect (fluid inertia or fluid elasticity), the grid resolutions used for calculating the rotation of the spheroid are approximately $\Delta = 1/32D_p$ for prolate spheroids in a Newtonian shear flow (Yu *et al.* 2007) and $\Delta = 1/16 \sim 1/42D_p$ for spheroids ($AR = 1.0$ and 4.0) in a viscoelastic shear flow (Krishnan *et al.* 2017; Wang *et al.* 2019; Rosti & Brandt 2020). Therefore, both the present convergence test and the previous studies indicate that the particle rotation modes obtained using the mesh with the present mesh resolution ($\Delta = 1/32D_p$) are reliable.

REFERENCES

ALTAN, M.C. 1990 A review of fiber-reinforced injection molding: flow kinematics and particle orientation. *J. Thermoplast. Compos.* **3** (4), 275–313.

ALVES, M.A., OLIVEIRA, P.J. & PINHO, F.T. 2021 Numerical methods for viscoelastic fluid flows. *Annu. Rev. Fluid Mech.* **53** (1), 509–541.

ATWELL, S., BADENS, C., CHARRIER, A., HELFER, E. & VIALLAT, A. 2022 Dynamics of individual red blood cells under shear flow: a way to discriminate deformability alterations. *Front. Physiol.* **12**, 775584.

BERIS, A.N., HORNER, J.S., JARIWALA, S., ARMSTRONG, M.J. & WAGNER, N.J. 2021 Recent advances in blood rheology: a review. *Soft Matt.* **17** (47), 10591–10613.

BIRD, R.B., CURTISS, C.F., ARMSTRONG, R.C. & HASSAGER, O. 1987 *Dynamics of Polymeric Liquids, Volume 2: Kinetic Theory*, 2nd edn. Wiley.

BRUNN, P. 1977 The slow motion of a rigid particle in a second-order fluid. *J. Fluid Mech.* **82** (3), 529–547.

CASTILLO, E. & CODINA, R. 2015 First, second and third order fractional step methods for the three-field viscoelastic flow problem. *J. Comput. Phys.* **296**, 113–137.

DABADE, V., MARATH, N.K. & SUBRAMANIAN, G. 2015 Effects of inertia and viscoelasticity on sedimenting anisotropic particles. *J. Fluid Mech.* **778**, 133–188.

DAGHOOGHI, M. & BORAZJANI, I. 2018 The effects of irregular shape on the particle stress of dilute suspensions. *J. Fluid Mech.* **839**, 663–692.

D'AVINO, G., GRECO, F. & MAFFETTONE, P.L. 2015 Rheology of a dilute viscoelastic suspension of spheroids in unconfined shear flow. *Rheol. Acta* **54** (11–12), 915–928.

D'AVINO, G., GRECO, F. & MAFFETTONE, P.L. 2017 Particle migration due to viscoelasticity of the suspending liquid and its relevance in microfluidic devices. *Annu. Rev. Fluid Mech.* **49** (1), 341–360.

D'AVINO, G., HULSEN, M.A., GRECO, F. & MAFFETTONE, P.L. 2014 Bistability and metabistability scenario in the dynamics of an ellipsoidal particle in a sheared viscoelastic fluid. *Phys. Rev.* E **89** (4), 043006.

D'AVINO, G., HULSEN, M.A., SNIJKERS, F., VERMANT, J., GRECO, F. & MAFFETTONE, P.L. 2008 Rotation of a sphere in a viscoelastic liquid subjected to shear flow. Part I: simulation results. *J. Rheol.* **52** (6), 1331–1346.

D'Avino, G. & Maffettone, P.L. 2015 Particle dynamics in viscoelastic liquids. *J. Non-Newtonian Fluid Mech.* **215**, 80–104.

Debbaut, B. & Crochet, M.J. 1988 Extensional effects in complex flows. *J. Non-Newtonian Fluid Mech.* **30** (2–3), 169–184.

Ding, E.-J. & Aidun, C.K. 2000 The dynamics and scaling law for particles suspended in shear flow with inertia. *J. Fluid Mech.* **423**, 317–344.

Ewoldt, R.H. & Saengow, C. 2022 Designing complex fluids. *Annu. Rev. Fluid Mech.* **54** (1), 413–441.

Fedosov, D.A., Pan, W., Caswell, B., Gompper, G. & Karniadakis, G.E. 2011 Predicting human blood viscosity in silico. *Proc. Natl Acad. Sci. USA* **108** (29), 11772–11777.

Gauthier, F., Goldsmith, H.L. & Mason, S.G. 1971 Particle motions in non-Newtonian media: I: Couette flow. *Rheol. Acta* **10** (3), 344–364.

Giesekus, H. 1982 A simple constitutive equation for polymer fluids based on the concept of deformation-dependent tensorial mobility. *J. Non-Newtonian Fluid Mech.* **11** (1–2), 69–109.

Gunes, D.Z., Scirocco, R., Mewis, J. & Vermant, J. 2008 Flow-induced orientation of non-spherical particles: effect of aspect ratio and medium rheology. *J. Non-Newtonian Fluid Mech.* **155** (1–2), 39–50.

Goldstein, H. 1980 *Classical Mechanics*, 2nd edn, pp. 143–148. Addison-Wesley.

Housiadas, K.D. & Tanner, R.I. 2011 The angular velocity of a freely rotating sphere in a weakly viscoelastic matrix fluid. *Phys. Fluids* **23** (5), 051702.

Huang, H., Yang, X., Krafczyk, M. & Lu, X.-Y. 2012 Rotation of spheroidal particles in Couette flows. *J. Fluid Mech.* **692**, 369–394.

Huang, W.-X., Chang, C.B. & Sung, H.J. 2011 An improved penalty immersed boundary method for fluid–flexible body interaction. *J. Comput. Phys.* **230** (12), 5061–5079.

Hwang, W.R., Hulsen, M.A. & Meijer, H.E.H. 2004 Direct simulations of particle suspensions in a viscoelastic fluid in sliding bi-periodic frames. *J. Non-Newtonian Fluid Mech.* **121** (1), 15–33.

Iso, Y., Cohen, C. & Koch, D.L. 1996a Orientation in simple shear flow of semi-dilute fiber suspensions 2. Highly elastic fluids. *J. Non-Newtonian Fluid Mech.* **62** (2–3), 135–153.

Iso, Y., Koch, D.L. & Cohen, C. 1996b Orientation in simple shear flow of semi-dilute fiber suspensions 1. Weakly elastic fluids. *J. Non-Newtonian Fluid Mech.* **62** (2–3), 115–134.

Jeffery, G.B. 1922 The motion of ellipsoidal particles immersed in a viscous fluid. *Proc. R. Soc. Lond.* A **102** (715), 161–179.

Johnson, S.J., Salem, A.J. & Fuller, G.G. 1990 Dynamics of colloidal particles in sheared, non-Newtonian fluids. *J. Non-Newtonian Fluid Mech.* **34** (1), 89–121.

Kang, I.S. 2002 A microscopic study on the rheological properties of human blood in low concentration limit. *Korea-Aust. Rheol. J.* **14** (2), 77–86.

Kim, K., Baek, S.-J. & Sung, H.J. 2002 An implicit velocity decoupling procedure for the incompressible Navier–Stokes equations. *Intl J. Numer. Meth. Fluids* **38** (2), 125–138.

Krishnan, S., Shaqfeh, E.S.G. & Iaccarino, G. 2017 Fully resolved viscoelastic particulate simulations using unstructured grids. *J. Comput. Phys.* **338**, 313–338.

Leal, L.G. 1975 The slow motion of slender rod-like particles in a second-order fluid. *J. Fluid Mech.* **69** (2), 305–337.

Li, G. & Ardekani, A.M. 2016 Collective motion of microorganisms in a viscoelastic fluid. *Phys. Rev. Lett.* **117** (11), 118001.

Li, G., McKinley, G.H. & Ardekani, A.M. 2015 Dynamics of particle migration in channel flow of viscoelastic fluids. *J. Fluid Mech.* **785**, 486–505.

Li, Y., Huang, W., Xu, C. & Zhao, L. 2022 An implicit conformation tensor decoupling approach for viscoelastic flow simulation within the monolithic projection framework. *J. Comput. Phys.* **468**, 111497.

Li, Z. & Lin, J. 2022 On the some issues of particle motion in the flow of viscoelastic fluids. *Acta Mechanica Sin.* **38** (3), 321467.

Lim, E.J., Ober, T.J., Edd, J.F., Desai, S.P., Neal, D., Bong, K.W., Doyle, P.S., McKinley, G.H. & Toner, M. 2014 Inertio-elastic focusing of bioparticles in microchannels at high throughput. *Nat. Commun.* **5** (1), 4120.

Lin, J. & Huo, L. 2015 A review of research on nanoparticulate flow undergoing coagulation. *Acta Mechanica Sin.* **31** (3), 292–302.

Liu, J., Li, C., Ye, M. & Liu, Z. 2020 The rotation of two-dimensional elliptical porous particles in a simple shear flow with fluid inertia. *Phys. Fluids* **32** (4), 043305.

Lu, X. & Xuan, X. 2015 Continuous microfluidic particle separation via elasto-inertial pinched flow fractionation. *Anal. Chem.* **87** (12), 6389–6396.

Lundell, F. & Carlsson, A. 2010 Heavy ellipsoids in creeping shear flow: transitions of the particle rotation rate and orbit shape. *Phys. Rev.* E **81** (1), 016323.

LUNDELL, F., SÖDERBERG, L.D. & ALFREDSSON, P.H. 2011 Fluid mechanics of papermaking. *Annu. Rev. Fluid Mech.* **43** (1), 195–217.

MAO, W. & ALEXEEV, A. 2014 Motion of spheroid particles in shear flow with inertia. *J. Fluid Mech.* **749**, 145–166.

NABERGOJ, M., UREVC, J. & HALILOVIČ, M. 2022 Function-based reconstruction of the fiber orientation distribution function of short-fiber-reinforced polymers. *J. Rheol.* **66** (1), 147–160.

NGO, T.T., NGUYEN, H.M.K. & OH, D.-W. 2021 Prediction of fiber rotation in an orifice channel during injection molding process. *J. Rheol.* **65** (6), 1361–1371.

NGUYEN-HOANG, H., PHAN-THIEN, N., KHOO, B.C., FAN, X.-J. & DOU, H.-S. 2008 Completed double layer boundary element method for periodic fibre suspension in viscoelastic fluid. *Chem. Engng Sci.* **63** (15), 3898–3908.

PAN, X., KIM, K.-H. & CHOI, J.-I. 2019 Efficient monolithic projection method with staggered time discretization for natural convection problems. *Intl J. Heat Mass Transfer* **144**, 118677.

PHAN-THIEN, N. & FAN, X.-J. 2002 Viscoelastic mobility problem using a boundary element method. *J. Non-Newtonian Fluid Mech.* **105** (2–3), 131–152.

PIMENTA, F. & ALVES, M.A. 2017 Stabilization of an open-source finite-volume solver for viscoelastic fluid flows. *J. Non-Newtonian Fluid Mech.* **239**, 85–104.

RAOUFI, M.A., MASHHADIAN, A., NIAZMAND, H., ASADNIA, M., RAZMJOU, A. & WARKIANI, M.E. 2019 Experimental and numerical study of elasto-inertial focusing in straight channels. *Biomicrofluidics* **13** (3), 034103.

ROSÉN, T., DO-QUANG, M., AIDUN, C.K. & LUNDELL, F. 2015*a* The dynamical states of a prolate spheroidal particle suspended in shear flow as a consequence of particle and fluid inertia. *J. Fluid Mech.* **771**, 115–158.

ROSÉN, T., DO-QUANG, M., AIDUN, C.K. & LUNDELL, F. 2015*b* Effect of fluid and particle inertia on the rotation of an oblate spheroidal particle suspended in linear shear flow. *Phys. Rev.* E **91** (5), 053017.

ROSÉN, T., LUNDELL, F. & AIDUN, C.K. 2014 Effect of fluid inertia on the dynamics and scaling of neutrally buoyant particles in shear flow. *J. Fluid Mech.* **738**, 563–590.

ROSTI, M.E. & BRANDT, L. 2020 Increase of turbulent drag by polymers in particle suspensions. *Phys. Rev. Fluids* **5** (4), 041301.

SAFFMAN, P.G. 1956 On the motion of small spheroidal particles in a viscous liquid. *J. Fluid Mech.* **1** (5), 540–553.

SNIJKERS, F., D'AVINO, G., MAFFETTONE, P.L., GRECO, F., HULSEN, M.A. & VERMANT, J. 2011 Effect of viscoelasticity on the rotation of a sphere in shear flow. *J. Non-Newtonian Fluid Mech.* **166** (7–8), 363–372.

SNIJKERS, F., D'AVINO, G., MAFFETTONE, P.L., GRECO, F., HULSEN, M. & VERMANT, J. 2009 Rotation of a sphere in a viscoelastic liquid subjected to shear flow. Part II. Experimental results. *J. Rheol.* **53** (2), 459–480.

STORM, C., PASTORE, J.J., MACKINTOSH, F.C., LUBENSKY, T.C. & JANMEY, P.A. 2005 Nonlinear elasticity in biological gels. *Nature* **435** (7039), 191–194.

TAYLOR, G.I. 1923 The motion of ellipsoidal particles in a viscous fluid. *Proc. R. Soc. Lond.* A **103** (720), 58–61.

VARCHANIS, S., TSAMOPOULOS, J., SHEN, A.Q. & HAWARD, S.J. 2022 Reduced and increased flow resistance in shear-dominated flows of Oldroyd-B fluids. *J. Non-Newtonian Fluid Mech.* **300**, 104698.

WANG, Y., YU, Z. & LIN, J. 2019 Numerical simulations of the motion of ellipsoids in planar Couette flow of Giesekus viscoelastic fluids. *Microfluid Nanofluid* **23** (7), 89.

YE, T., PHAN-THIEN, N. & LIM, C.T. 2016 Particle-based simulations of red blood cells—a review. *J. Biomech.* **49** (11), 2255–2266.

YU, Z., PHAN-THIEN, N. & TANNER, R.I. 2007 Rotation of a spheroid in a Couette flow at moderate Reynolds numbers. *Phys. Rev.* E **76** (2), 026310.

YU, Z., WANG, P., LIN, J. & HU, H.H. 2019 Equilibrium positions of the elasto-inertial particle migration in rectangular channel flow of Oldroyd-B viscoelastic fluids. *J. Fluid Mech.* **868**, 316–340.